Biorenewable polymer thermoplastic biocomposites

by

Mitchel Mathew Michel

A thesis submitted to the graduate faculty

in partial fulfillment of the requirements for the degree of

MASTER OF SCIENCE

Major: Industrial and Agricultural Technology

Program of Study Committee:
David Grewell, Co-major Professor
Reza Montazami, Co-major Professor
Thomas Brumm

The student author, whose presentation of the scholarship herein was approved by the program of study committee, is solely responsible for the content of this thesis. The Graduate College will ensure this thesis is globally accessible and will not permit alterations after a degree is conferred.

Iowa State University

Ames, Iowa

2018

TABLE OF CONTENTS

Page

LIST OF FIGURES

LIST OF TABLES

NOMENCLATURE

AF	Agave Fibers
CHO	Carbohydrates
HDPE	High-density Polyethylene
HPL	Hydroxypropyl Lignin
LLDPE	Linear Low-density Polyethylene
MA	Maleic Anhydride
PP	Polypropylene
PPr	Rhetech Polypropylene
SEM	Scanning Electron Microscope
AF	Thermoplastic Composite

ACKNOWLEDGMENTS

I would like to thank my Fiancée Jessica and son Mathias for their relenting support at home during my degree. They continue to provide me with motivation and a purpose for the success of my future.

A sincere thanks to my immediate family including my parents John and Denise, and my seven siblings Joshua, Danielle, Manessa, Jenna, John, ad Daniel for helping to instill in me the farmers hard work ethic and principal understanding of striving to continually improve yourself.

I would like to give credit to my research mentors Dr. David Grewell, Dr. Reza Montazami, and Dr. Thomas Brumm for their continued guidance throughout the entirety of my academic journey.

I would like to thank then Center for Bioplastics and Biocomposites, the National Science Foundation, and the many Industry partners for their support in funding to make this research possible.

I would like to give credit to the many researchers Jake, Mellisa, Matt, Brian, Samantha and the many others that assisted in the experimental processes. I experienced the true definition of teamwork towards my completion.

ABSTRACT

Biorenewable fillers have recently gained a greater focus in research to produce composites because of their unique properties, abundance, and diversity. These biorenewable fillers can include various terrestrial based plants naturally grown throughout the world. The focus of this work was on the natural fiber feedstocks that are created as waste streams from a wide range of industries, in particular agave fibers. Creating a composite composed of fibrous materials would have potential benefits that include cutting costs of composite products, decrease in density, increased strength and durability, and utilizing plant fiber waste streams for cost recovery. However, these natural fibers tend to be hydrophilic in nature and do not adhere well to hydrophobic polymer matrices. Directly combining plant fibers with plastics tends to yield poor mechanical properties because of this incompatibility. These plant fibers must first go through treatment(s) to alter their surface properties, mechanically and/or chemically, to promote strong interfacial bonding to occur.

Processing temperatures of polymers for extrusion or molding into a finished part vary based on the polymer used; however, they tend to be higher than the degradation temperatures of the fibers, which can result in brittle fibers. Polymers such as polyethylene and polypropylene have processing temperatures ranging from 140-200 °C. To allow processing of fiber-reinforced composites, polymer additives are used to suppress the processing temperatures and thus reduce thermal degradation of the natural fibers. Finding both ideal treatments for fibers and additives for polymers will allow a wide variety of feedstocks to be utilized throughout the world, affecting many industries. Potential industries impacted by this research include automotive, aerospace, and consumer goods.

Early success has been observed in creating biofilled composites displaying significantly improved mechanical properties. Creating functionalized chemical bonding groups to promote surface interactions of biofibers and polymer matrices is important to enhance the properties of these composites. In this project, modified lignin and agave fibers were utilized as fillers in biocomposites with high-density polyethylene (HDPE), linear low-density polyethylene (LLDPE), and polypropylene (PP), as the matrix polymers. It was found that with proper pretreatments and processing conditions, it is possible to produce biocomposites with higher specific strength (strength: density) compared to traditional composites, such as glass reinforced composites. It was also seen that at higher filler levels (20-25%), the mechanical properties were maximized as a result of fiber to fiber interaction and entanglement.

CHAPTER 1. INTRODUCTION

Bioplastics

Plastics are used in numerous applications based upon their wide range of inherent properties which in turn depend on the base polymer(s). For applications that demand a high degree of flexibility, e.g., from thin film expanding trash bags to 30-gallon garbage bags, plastics such a polythene (PE) are well suited. Commodity plastics such as polyethylene and polypropylene are excellent examples of plastics with thermo-mechanical properties able to meet the needs of many applications; however, many factors can influence these properties, such as processing and addition of fillers. Notably high performing plastics such as polybenzimidazole (PBI), better known by the trade name Celazole, meet the requirements of high performance applications within the aerospace industry because of their impact and tensile strength, hardness, shear strength, and wear resistance under thermally stressed conditions with a glass transition temperature of 417 °C [1]. Plastics, including those previously stated, are defined as being man-made polymers. Polymers are by definition, many (*poly*) repeating units (*mers*), which make chains of thousands of repeating units. Polyethylene, a common commodity plastic, for example, is comprised of repeating ethylene units as seen in Figure 1.1 [2]. The configuration of these polymer chains, the number of repeating units (*n*) (or its molecular weight), the side chain functionality, as well as processing conditions greatly influences the thermo-mechanical properties of the material.

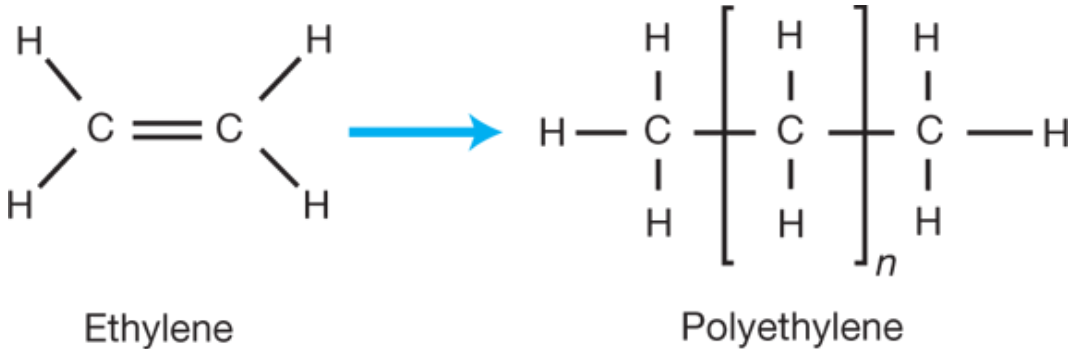

Figure 1.1 *Molecular structure of ethylene monomer (left) and polyethylene (right)*

The back bones of long polymer chains are held together with primary carbon-carbon covalent bonds, while the bulk of polymer chains are held together by entanglement forces, e.g., van der Waals forces, hydrogen bonding, and dipole-dipole interactions, which restrict the chains' ability to slide past each other, which is why polymer chains often compared to a bowl of cooked spaghetti noodles.

Plastics, which maybe consider man-made polymers derived from petrochemical feedstocks, first saw mass production in the 1940s. Because modern plastics are synthesized, nature lacks natural pathways necessary to degrade these polymers, posing threats to earth's ecosystem. However, there are also polymers found in nature including proteins, starches, and DNA. Being found in nature, these polymers provide pathways for organisms to degrade them. In addition, it is possible to use feedstocks such as corn, vegetable oils, soybeans, and sugar cane are commonly to derive bioplastics. Bioplastics, being derived from natural monomers, can – but may not always – be readily degraded by organisms. This hierarchy of classification is better explained in Figure 1.2 [3].

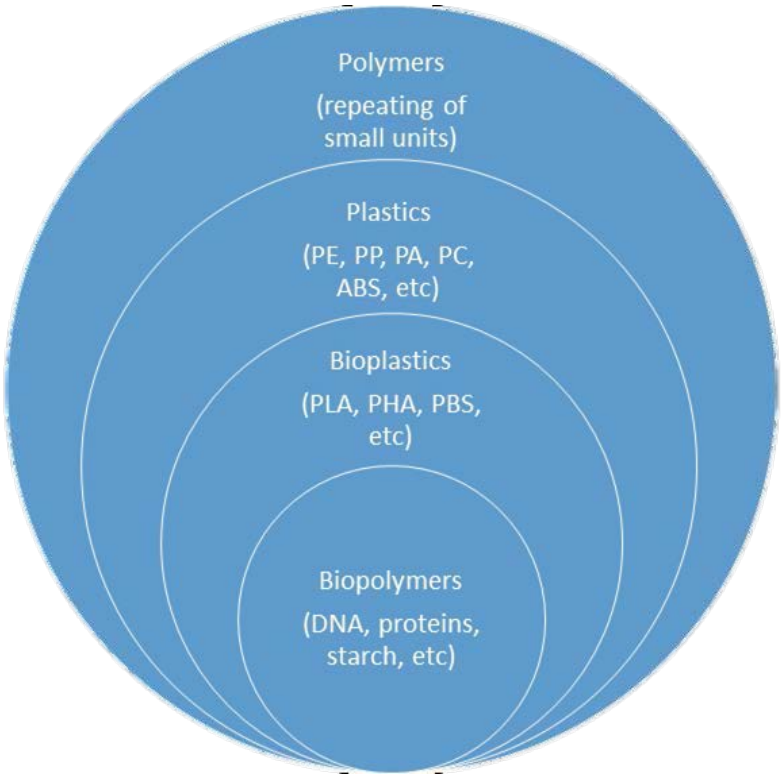

Figure 1.2 *Hierarchy of polymer classes*

Polymers are categorized by three polymer morphologies: amorphous, semi-crystalline, and cross linked, as seen in Figure 1.3 [3], each having different molecular configurations. In amorphous and semi-crystalline, relatively week secondary forces can be easily broken through external forces such as temperature and/or shear, they are classified as thermoplastics. These external forces allow polymer chains to flow or to be plasticized. Thermoplastics do not flow like water but display viscoelastic properties similar to Silly-Putty® that are dependent on the flow rate as well as temperature. Using these principles, thermoplastics can be plasticized multiple times to make new geometries/parts.

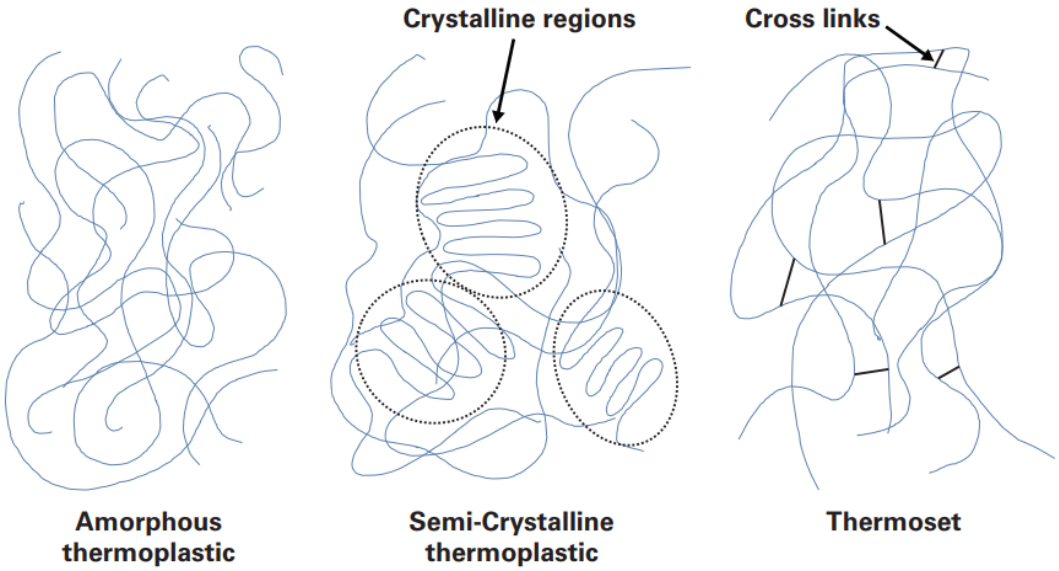

Figure 1.3 *Possible configurations of polymer morphologies*

Cross linked polymers, referred to as thermosets, are comprised of long polymer chains, similar to the amorphous and semi-crystalline polymers; however, they are bridged/linked together through a network of cross linking molecules. These networks, formed during the synthesis process, form strong covalent bonds, similar to the primary bonds of polymer chain backbones. Thermosets tend to be relatively thermally stable because of these cross-links and, unlike thermoplastics, the polymer chains are not able to slide past each other in a plasticization process (heating). With the introduction of heat, thermosets do not plasticize and flow, instead the polymer chains will thermally degrade once sufficiently heated.

The physical properties associated with polymers can vary and are better represented by comparing and contrasting the stress (σ)/strain (ε) curves as seen for various classes of plastics in Figure 1.4 [3]. Brittle plastics tend to exhibit relative high stresses before failure. In contrast, elastomeric plastics (rubbery) tend to have low strengths and

deform easily under stress, exhibiting high elongation before failure. Ductile plastics fall between these two and are able to sustain relatively high stress loads while experiencing some elongation and deformation before failure. From these stress-strain curves, material properties such as Young's modulus or stiffness of a material, percent elongation, ultimate stress or strength, toughness, and the yielding stress or strength of the plastics, can be determined.

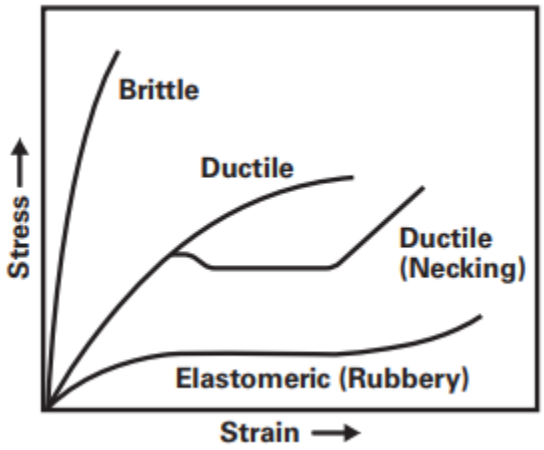

Figure 1.4 *Stress-Strain curves of plastics* **[3]**

Polymer materials' properties, as previously stated, can vary greatly based upon the polymer's chemical structure and processing. However, a polymer consisting of a single repeating monomer, known as a homopolymer, can have a limited range of properties. The possible variations in mechanical properties are limited only to varying molecular weight and processing conditions.

However, polymers are not restricted to being homopolymers, but can take varying forms through the combination of two or more varying monomers, also called copolymers. Copolymer structures of desired monomer configurations can be induced under the correct conditions and synthesized at an industrial scale. These copolymer structures may be of

various morphologies belonging to four categories: random, alternating, block, or graft as seen in Figure 1.5 [4]. The resulting copolymers exhibit combined properties of the base homopolymers, yielding enhanced polymers.

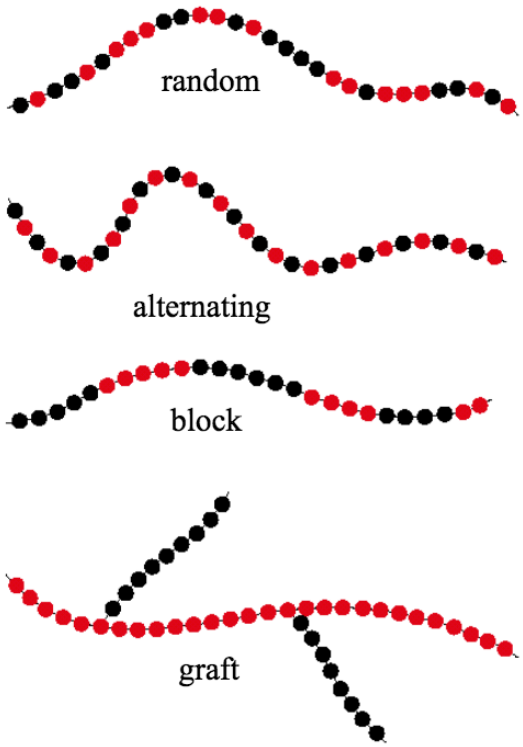

Figure 1.5 *The four basic copolymer morphologies*

In addition to synthesis co-polymerization, it is also possible to compound two or more polymers together to produce blends that exhibit enhanced properties compared to either base polymer.

Composites

Composite materials consist of two or more distinct phases of base/primary materials: A primary phase consisting of a matrix polymer and a secondary phase consisting of a reinforcing filler. Composites' properties reflect the properties of both phases and are primarily created to improve strength, stiffness, and/or density. The matrix

serves several functions for the composite, such as providing the bulk form of the composite, binding the filler, and allowing the forces to be distributed and shared within the composite. Composites can be classified under into two categories, traditional and synthetic. Traditional composites are those occurring in nature such a trees or natural fibers. Synthetic composites feature a man-made plastic and either a natural or a synthetic filler, such as glass or carbon fibers.

Fibers

Fibers are filaments used as reinforcing materials; they can be circular, rectangular, tubular, and hexagonal in cross section. Fiber reinforcement in composites provides great opportunities for the overall enhancement of the composite material's properties as the fibers are often inherently stronger compared to the bulk polymer matrix. The effects of fiber diameter can also attribute to the strength of the composite. As fiber diameter is reduced, the fibers become more flexible and can readily align along the principal axis of flow during composites forming. Fiber composites are classified into two groups, continuous and discontinuous fiber composites. Continuous fibers have long aspect ratios (length/diameter) and provide continuous reinforcement to enhance mechanical properties. Discontinuous fibers are short fibers with aspect ratios of 100 or less. In both cases the fibers can have either a predetermined or random orientation.

Particles

Particles are another common filler for composite materials. Particles may vary in size from the microscopic to the macroscopic range (1 nm – 20,000 nm). The distribution of particles throughout a matrix polymer is random and therefore the composite will tend to have isotropic properties. Dispersed particles within matrices at 15% loading do not

distribute stress in the composite [4] because of their short length/size. However, they tend to promote strength and hardening of the matrix polymer by restricting polymer chain mobility and thereby strengthening the polymer matrix. As particle sizes increase and loading increases above 25%, the properties can change within the composite [4]. Applied stresses on the composite structure are shared because the relatively high strength of the particles and proper bonding between the polymer matrix and the filler.

Rule of mixtures for density

Composite materials' properties are functions of the base materials. Properties of these composites can be calculated using the rule of mixtures. The rule of mixtures is a calculated weighted average of the base materials. Density is one example of a property calculated by the rule of mixtures. The mass of a composite is the sum of the masses of the matrix polymer and the reinforcing filler as seen in Equation 1.

$$m_c = m_m + m_f$$

Equation 1

Where the mass of the composite (m_c) is equal to the sum of the mass of the polymer matrix (m_m) and the fiber mass (m_f). The volume of composites can also be calculated as the sum of base materials as seen in Equation 2.

$$V_c = V_m + V_f + V_v$$

Equation 2

Where the volume of the composite (V_c) is equal to the sum of the volume of matrix polymer (V_m), the volume of the fiber (V_f), and the volume of voids (V_v). Assuming no voids, the density of composites can also be calculated as the mass divided by volume as seen in Equation 3.

$$\rho_c = \frac{m_c}{V_c} = \frac{m_m + m_f}{V_c}$$

Equation 3

Where the density of the composites (ρ_c) is equal to the mass of the composite divided by the volume of the composite. The masses of the matrix and filler are calculated as their densities multiplied by their volumes as seen in Equation 4 and Equation 5.

$$m_m = \rho_m V_m$$

Equation 4

$$m_f = \rho_f V_f$$

Equation 5

Substituting Equation 4 and Equation 5 into Equation 3 gives us the resulting equation:

$$\rho_c = f_m \rho_m + f_f \rho_f$$

Equation 6

Where the (f_m) and (f_f) are the volume fractions of the polymer matrix and filler respectively.

Theory of composites

As previously stated, composites are used to produce materials with higher mechanical properties compared to traditional materials. While ultimate strength is often the primary property that is considered when developing composites, estimating the ultimate strength can be challenging because it is highly dependent on the interfacial strength of the filler and the matrix. However, with relatively long or continuous unidirectional fibers it is possible to estimate the stiffness of composite in both the longitudinal and transverse directions.

Stiffness of composites in the longitudinal direction

In the longitudinal direction, the applied force is in parallel to the direction of the fibers in a unidirectional continuous fiber composite, as seen in Figure 1.6.

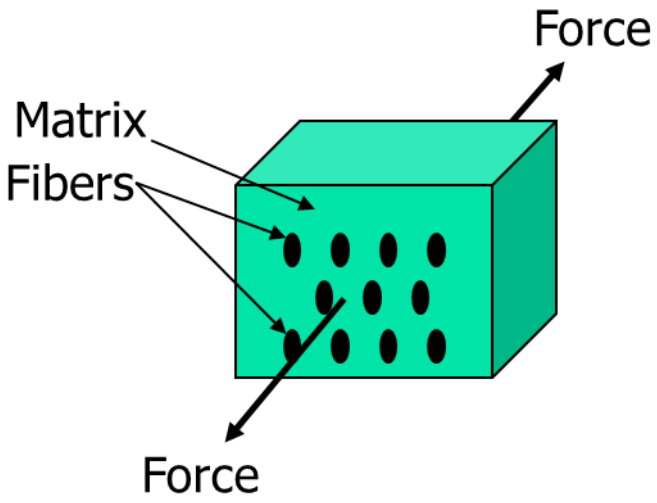

Figure 1.6 *Schematic of longitudinal loading of a unidirectional continuous fiber composite*

It is possible to remove an imaginary unit cell from the composite that has the same volume fraction of matrix (V_m) and fiber volume fraction (V_f) as the composite, as seen in Figure 1.7.

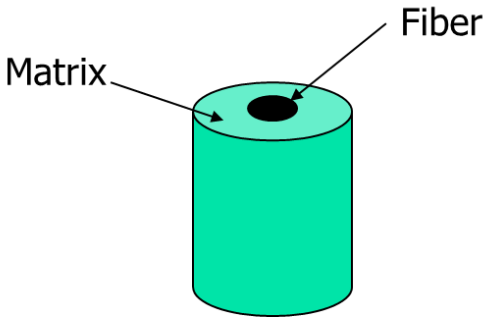

Figure 1.7 *Schematic of volume removed from the composite in longitudinal loading*

If it is assumed that the element is sufficiently long, the strain (ε) in the fiber (ε_f), matrix (ε_m), and composite(ε_c) are equal as seen in Equation 7.

$$\varepsilon_f = \varepsilon_m = \varepsilon_c = \varepsilon$$

Equation 7

Under this equilibrium condition, it is possible to derive a relationship for the composite force (F_c) based on the forces in the matrix (F_m) and fiber (F_f), as shown in Equation 8.

$$F_c = F_m + F_f = A_m\sigma_m + A_f\sigma_f$$

Equation 8

Where (A_m) and (A_f) are the cross-sectional areas of the matrix and fiber, respectively, which are directly proportional to the volume fraction of each component, as seen in Equation 9.

$$F_c = A_m\sigma_m + A_f\sigma_f = A_mE_m\varepsilon + A_fE_f\varepsilon = \varepsilon\left(A_mE_m + A_fE_f\right)$$

Equation 9

In Equation 9, E is the modulus of each components. By dividing Equation 8 by the total area of the element (A_c) it is possible to derive a relationship for the longitudinal modulus for the composite (E_c) based on the filler level and know modulus of the matrix as seen in Equation 10.

$$\frac{F_c}{A_c} = \varepsilon\left(\frac{A_m}{A_c}E_m + \frac{A_f}{A_c}E_f\right)$$
$$\sigma_c = \varepsilon\left(V_mE_m + V_fE_f\right)$$
$$\frac{\sigma_c}{\varepsilon} = \frac{\varepsilon}{\varepsilon}\left(V_mE_m + V_fE_f\right) = E_c = V_mE_m + V_fE_f$$

Equation 10

This is another example of the rule of mixture.

Stiffness of composites in the transverse direction

In the transverse loading condition, the loads are perpendicular to the fiber of a unidirectional continuous fiber composite, as seen in Figure 1.8.

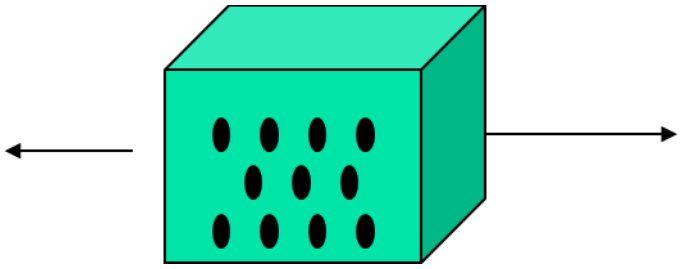

Figure 1.8 *Schematic of unidirectional continuous fiber composite in a transverse loading condition*

Again, it is possible to remove an imaginary unit cell from the composite that has the same volume fraction of matrix (V_m) and fiber volume fraction of fiber (V_f) as the composite, as seen in Figure 1.9.

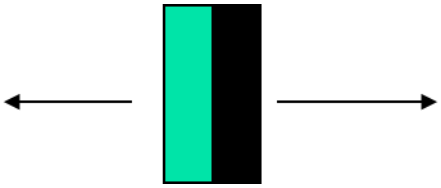

Figure 1.9 *Schematic of volume removed from the composite in transverse loading condition*

In this case, the stress for the matrix (σ_m), fiber (σ_f) and composite (σ_c) are all equal. In addition, the summation strain of the fiber (ε_f) and the matrix (ε_m) equal the strain of the composite (ε_c), as seen in Equation 11.

$$\varepsilon_c = \varepsilon_f + \varepsilon_m$$

Equation 11

It is possible to use a transfer function that correlates the stiffness of each component to a spring with a stiffness (K), as seen in Figure 1.10.

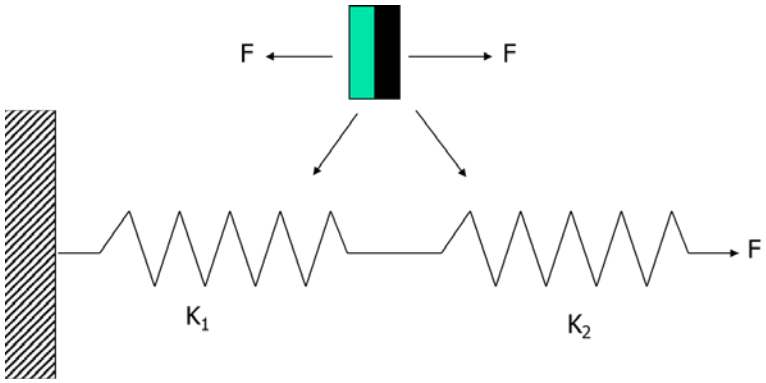

Figure 1.10 *Schematic of spring representation of an element from transverse loaded composite*

Where (K_1) and (K_2) are the spring stiffness coefficients of each spring. In this model, the stiffness of two springs in series (K) as seen in Figure 1.10, is defined in Equation 12.

$$\frac{1}{K} = \frac{1}{K_1} + \frac{1}{K_2}$$

Equation 12

Knowing the stiffness of each component, (K) can be modeled as seen in Equation 13.

$$K = \frac{E_1 A}{L_1}$$

Equation 13

It is possible to determine the overall stiffness of the composites. In this case, the volumetric fraction is directly proportional to the length (L) of the model (width in Figure 1.9). Substituting Equation 13 in Equation 12 it is possible to derive Equation 14.

$$\frac{L_c}{E_c A} = \frac{L_f}{E_f A} + \frac{L_m}{E_m A}$$

Equation 14

Multiplied by the area (A), Equation 14 can be simplified as seen in Equation 15.

$$\frac{L_c}{E_c} = \frac{L_f}{E_f} + \frac{L_m}{E_m}$$

Equation 15

By dividing Equation 15 by entire length of the element (L_c) and assuming the lengths are equal to the volume fraction, it is possible to define the transverse modules of the composite, as seen in Equation 16.

$$\frac{1}{E_c} = \frac{V_f}{E_f} + \frac{V_m}{E_m}$$

Equation 16

Biocomposites

Biocomposites, as the name implies, are comprised of either bio based or non-man (synthetic) made materials forming the polymer matrix, the filler materials, and in some cases both. Matrix polymers may be petroleum-derived such as PP and PE, or biodegradable such as polylactic acid (PLA) and polyhydroxyalkanoate (PHA). Filler materials may be synthetic such as E-glass, or natural fibers or particles such as agave fibers and lignin, the focus of our studies. Composite having at least one portion being bio based is a biocomposite.

CHAPTER 2. RESEARCH QUESTION

In this research, biocomposite materials were developed, consisting of PP, HDPE, and LLDPE polymer matrixes reinforced with fillers including lignin and agave fibers. Polypropylene (PP) and PE are commonly used commodity plastics in the manufacturing of injection molded parts and assembly components. Automotive manufacturers are seeking alternative paths to decrease their carbon footprint while improving performance and increase consumer popularity of their production by incorporating natural material feedstocks and coproducts into their processes.

The Center for Bioplastics and Biocomposites (CB^2), a National Science Foundation Industry & University Cooperative Research Center (I/UCRC), served as a catalyst for this research. Partnering with industry members, coproducts such as lignin and agave fibers were identified as underutilized, low-cost coproducts currently being burned or landfilled.

This research tested the thermomechanical effects of lignin and agave fibers as fillers in commodity thermoplastic composite structures and compared them against their base polymer matrix. These natural fillers, when compounded with a polymer matrix, can form a composite material suitable for the replacement of current composite materials used by the automotive industry.

In addition, the organic compound maleic anhydride was incorporated as a compatibilizer between the polymer matrix and the reinforcing fillers. Maleic anhydride grafted polymers can react with hydroxyl groups on the surface of the fillers. These

reactions can form hydrogen or covalent bonds, leading to improved tensile strength, stiffness, and impact strength of the resulting matrix composites [5].

It was hypothesized through this research that suitable biocomposite materials constituting lignin or agave fibers as fillers can be manufactured using thermal extrusion and injection molding processes to produce components with thermomechanical properties suitable for the automotive industry. Thus, the broad reaching research question, is “Can biocomposites be developed that can have superior thermal mechanical properties compared to traditional composites?”

CHAPTER 3. LIGNIN THERMOPLASTIC COMPOSITES

Journal article for presentation to the Journal of Polymer Science

Mitchel Michel[a], Alper Kiziltas[b], Richard Hoch[c], Kevin Weiss[d], Nhiem Cao[e], David Grewell[a], Reza Montazami[f]

[a] Agricultural and Biosystems Engineering, Iowa State University, Ames, IA 50011, USA

[b] Ford Motor Company, Dearborn, MI 48120, USA

[c] Diageo, London, NW10 7HQ, UK

[d] Byogy, San Jose, CA 95110, USA

[e] Cyclewood, Fayetteville, AR 72701, USA

[f] Department of Mechanical Engineering, Iowa State University, Ames, IA 50011, USA

Objectives

The objectives of this study were to:

1. Develop a low-cost, biobased lignin composite to serve as a “one-to-one drop-in” for traditional plastics and/or plastic composites.
2. Develop biobased composites formulations that have enhanced mechanical properties, namely tensile strength and stiffness.
3. Develop a pretreatment and/or compatibilizer to improve filler-matrix bonding.
4. Identify proper compounding and injection molding processing conditions for biobased composites to enhance thermal-mechanical properties.
5. Analyze the mechanical properties, performance, and density of biobased composites.

6. Characterize biobased filler-matrix interfacial bonding using scanning electron microscopy.
7. Provide design recommendations for biobased composite products/components.

Introduction

The most accepted definition of biocomposites is attributed to Mohanty [6] and states that a biocomposite falls into two categories. The first, biocomposites are derived from natural fibers with petroleum polymer matrices, which is the focus of this study. The second, biocomposites are defined as being derived from plant based polymers with synthetic fillers. Of course, it is possible to create a fully biocomposite, with both filler and matrix being biobased.

Biofibers can be naturally grown plant fibers from both woody and non-woody feedstocks that are comprised of cellulose, lignin, and protein. Cellulose is a natural hydrophilic polymer consisting of d-anhydroglucose ($C_6H_{11}O_5$) repeating units joined by 1,4-β-d-glycosidic linkages at the C_1 and C_4 position [7]. Each repeating unit contains three hydroxyl groups with the ability to form hydrogen bonds governing the crystalline structures. While cellulose is resistant to alkali, it is easily hydrolyzed to water-soluble sugars with acid [8]. Lignin is a natural, amorphous, hydrophobic, complex hydrocarbon polymer with a high molecular weight. The exact chemical nature of lignin has not yet been determined but is known to contain five hydroxyl and five methoxyl groups per building unit [8]. Lignin functions as a filler of cellulose, stiffening cell walls and protecting against physical and chemical degradation [6].

Biocomposites containing biofibers have a variety of applications and have seen growth in the domestic sector, building materials, aerospace industry, electronics industry,

and automotive applications in the past decade [9]. Cellulose and lignin are readily available and abundant in nature and agricultural industry as inexpensive products and byproducts from current industries. Tensile strengths and Young's moduli of natural fibers are lower compared to synthetic fibers such as E-glass, but specific moduli (property/density) and stiffness are comparable, making them ideal replacements that result in lighter products [6].

Separating cellulose and lignin yields two very different physical and chemical polymers which will be discussed later. However, an efficient method for separating them with high yields has yet to be found and this added step increases the overall resulting costs. Thus, based on current technologies, utilizing whole plant fibers is economically advantageous. Lignocellulosic plant fibers, given their polarity and hydrophilic nature, compounded with non-polar hydrophobic thermoplastics, such as polyethylene and polypropylene, result in poor interfacial bonding. However, high interfacial bonding is crucial to produce high-strength composites that evenly distribute stress between the fibers and the polymer matrix. Pre-treatments to biofibers and thermoplastic matrix are required to promote stronger interfacial bonds.

Experimental

Materials

The lignin used in this study was hydroxypropyl lignin (HPL), an alkali supplied by Cyclewood (Dallas, Texas) in dry powder form. The compatibilizer, maleic anhydride (MA), had a molecular weight of 98.06 g/mol (Sigma-Aldrich). The thermoplastic matrix materials used in this study included a high-density polyethylene (HDPE), linear low-density polyethylene (LLDPE), polypropylene (PP), and polypropylene-r (PPr). The HDPE

had a melt flow index of 20 g/10 min at 190 °C and a density of 0.952 g/cm^3 (Chevron Phillips Chemical Company LP, Texas). The LLDPE had a melt flow index of 20 g/10 min at 190 °C and a density of 0.925 g/cm^3 (ExxonMobil Chemical Corporation, Texas). The PP had a melt flow index of 20 g/10 min at 230 °C and a density of 0.868 g/cm^3 (Formosa Plastics Corporation, Texas). The polypropylene (PPr) had a melt flow index of 34 g/10 min at 230 °C and a density of 0.91 g/cm^3 (Asahi Kasei Plastics Corporation, Michigan).

Co-extrusion of HPL and thermoplastics

Matrix polymers were melt blended with HPL lignin in a Leistritz 18 mm co-rotating twin-screw extruder with a barrel – l/d ratio of 25:1. The temperature profiles (°C) and extrusion speeds (RPM) used for the compounding are detailed in Table 3.1.

Table 3.1 *Thermal extrusion temperature profiles (°C) and speed parameters (RPM)*

Heating Zones		*1 (hopper)*	*2*	*3*	*4*	*5*	*6*	*Screw Speed (RPM)*
Resin	LLDPE	165	175	180	175	170	165	250
	HDPE	175	180	185	185	180	170	225
	PP	190	210	215	215	200	190	170
	PP-r	195	210	215	220	215	210	275

Materials were fed to the extruder using a Schenck AccuRate volumetric feeder with speeds of 100-200 RPM on a 0-999 scale. For all given formulations, batch size was 250 g to minimize HPL and MA powder settling inside the AccuRate. The lignin was ground to particle sizes <50 μm with mortar and pestle. Particle sizes were measured using a digital optical microscope. Materials were premixed and fed simultaneously into extruder zone 0. The formulations compounded are detailed in Table 3.2. For each of the

formulations detailed in Table 3.2, ten replicate tensile specimens were produced. Replicated formulations underwent an additional extrusion cycle to test the effects of secondary extrusion on mechanical properties.

Table 3.2 *Formulation details of HDPE, LLDPE, PP, and PPr composites*

Base Resin	*% Resin*	*% Filler*	*% Maleic Anhydride*	*Base Resin*	*% Resin*	*% Filler*	*% Maleic Anhydride*
HDPE	100	0	0	**LLDPE**	100	0	0
	95	5	0		95	5	0
	90	10	0		90	10	0
	85	15	0		85	15	0
	80	20	0		80	20	0
	70	30	0		70	30	0
	60	40	0		60	40	0
	94	5	1		94	5	1
	89	10	1		89	10	1
	83.5	15	1.5		83.5	15	1.5
	78.5	20	1.5		78.5	20	1.5
	68	30	2		68	30	2
					58	40	2
PP	100	0	0	**PPr**	100	0	0
	95	5	0		95	5	0
	90	10	0		90	10	0
	85	15	0		85	15	0
	80	20	0		80	20	0
	94	5	1		94	5	1
	89	10	1		89	10	1
	83.5	15	1.5		83.5	15	1.5
	78	20	2		78	20	2

Injection molding of test specimens

A BOY 22S, 28-mm injection molding machine was used to mold tensile test specimens from the various formulations. The temperature profiles utilized are detailed in Table 3.3.

Table 3.3 *Thermal injection molding temperature profiles (°C).*

Heating Zone		*1 (hopper)*	*2*	*3*	Mold Temp
Resin	LLDPE	175	180	170	45
	HDPE	180	185	175	52
	PP	190	210	190	52
	PP-r	190	210	190	52

Morphology

Scanning electron microscope (SEM) images were taken of tensile test fracture surfaces to characterize the effects of the maleic anhydride as a compatibilizer. Sample fracture surfaces were not sputter coated prior to SEM preparation as this was only for qualitative analysis, and only relatively low magnifications were used in an environmental SEM. This also allowed back scatter characterization of the chemical composition of the surfaces.

Tensile test

Tensile tests were conducted according to ASTM D638-14 [10] for Type I specimens with a testing speed of 50 mm/min. The ultimate tensile strength (UTS), 0.2% yielding strength, Young's modulus, and percent elongation at peak stress were calculated from a constant cross head displacement for 10 specimens within each sample group. Cross sectional area of specimens was calculated prior to test with a Fowler electronic caliper and assumed constant throughout testing. This assumption was then used to determine the percent elongation absent an extension meter.

Density test

The average densities of the composites were determined from dry initial weights and immersion of thermally compounded pelletized samples. Dry convection oven sample

weights were measured and recorded. Samples were then submerged into 2-propanol and volumetric displacement measured within a graduated cylinder. The average density was calculated as defined in Equation 18, where (ρ_c) is the composite density, (m) is the dry mass of the composite sample, (V_i) is the initial volume, and (V_f) is the final volume measured within the graduated cylinder after composite was inserted.

$$\rho_b = \frac{m}{V_f - V_i}$$

Equation 17

Results and Discussion

Morphology

Figures 3.1.a-d and 3.2.a-d display images of PP biocomposites with 5% and 20% HPL filler content with and without maleic anhydride, respectively. Figure 3.1 shows that without MA, isotropic PP thermoplastic composites (TPC) at 5% and 20% HPL exhibited HPL particles ranging in size between 1-5 µm. However, there were some HPL particles ~50 µm in size which was most likely the result of uneven mortar and pestle grinding as seen in Figure 3.1b and Figure 3.1d. In addition, voids were present between HPL particles at 5% filler content, as seen in Figure 3.1a. At a higher HPL content of 20%, these voids occurred more frequently, as seen in Figure 3.1c. In comparison, Figure 3.2 shows an isotropic PP TPC comprised of HPL-MA at 5:1 and 20:2 ratios, respectively, with aggregate particle sizes ranging from ~10-100 µm. Figure 3.2a and Figure 3.2c (in rectangles) show a correlation between increased MA and HPL content and increased HPL agglomerates. Similarly, voids were present between HPL particles at 5% and 20% filler content, as seen circled in Figure 3.2a-b and Figure 3.2c-d, respectively. Both TPCs SEM images revealed voids between HPL particles and the PP matrix. These voids suggest

limited bonding between the PP polymer matrix and the HPL filler, even with the addition of the MA compatibilizer. Thus, there is no evidence that MA increases interfacial bonding between PP and HPL. It is also seen that MA may promote the agglomeration of the HPL filler, limiting the enhancement of mechanical properties.

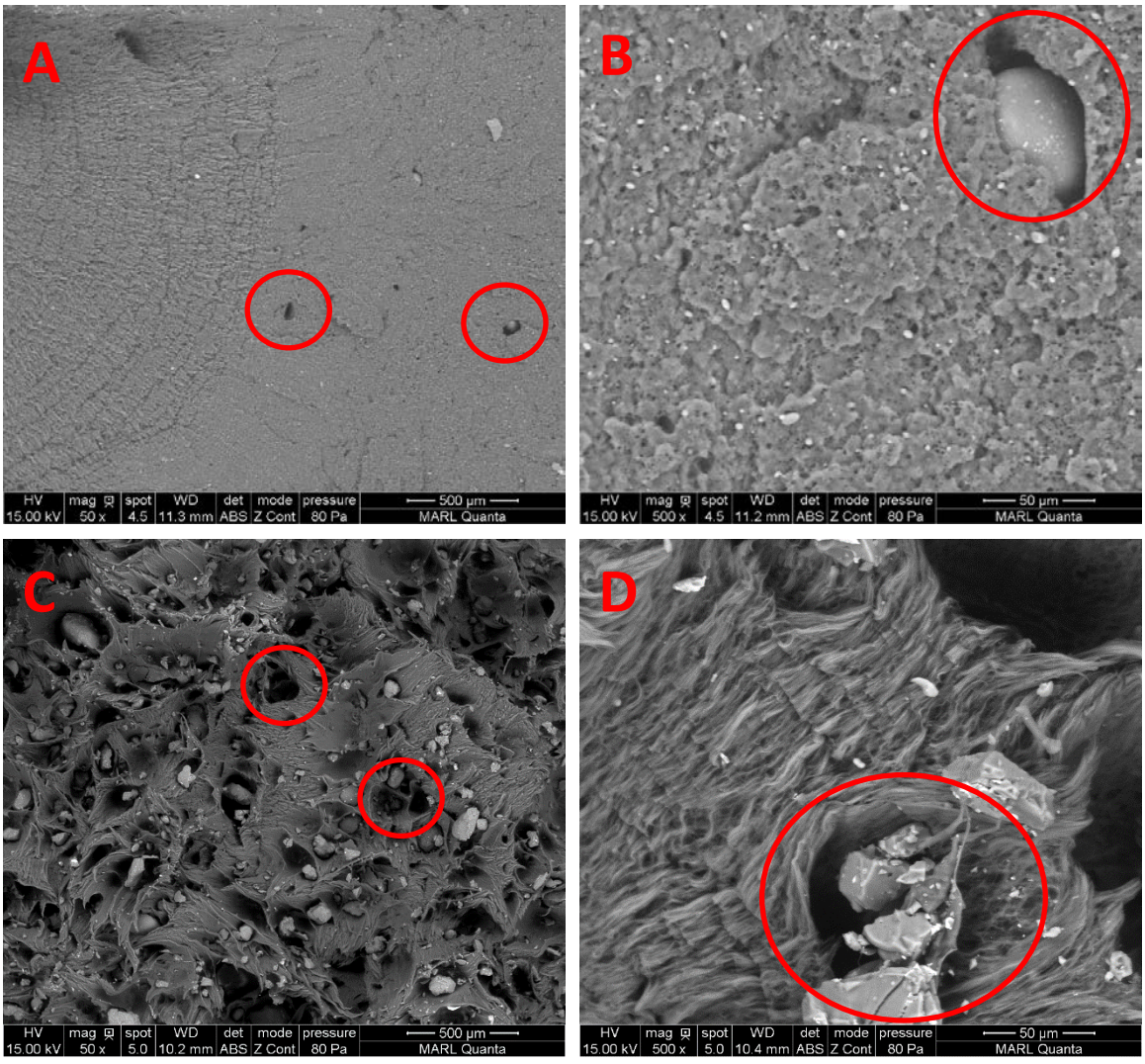

Figure 3.1 *SEM of tensile specimen fracture surface of PP-HPL 95/5 single extrusion at 50x magnification (a) and 500x magnification (b); PP-HPL 80/20 single extrusion at 50x magnification (c) and 500x magnification (d).*

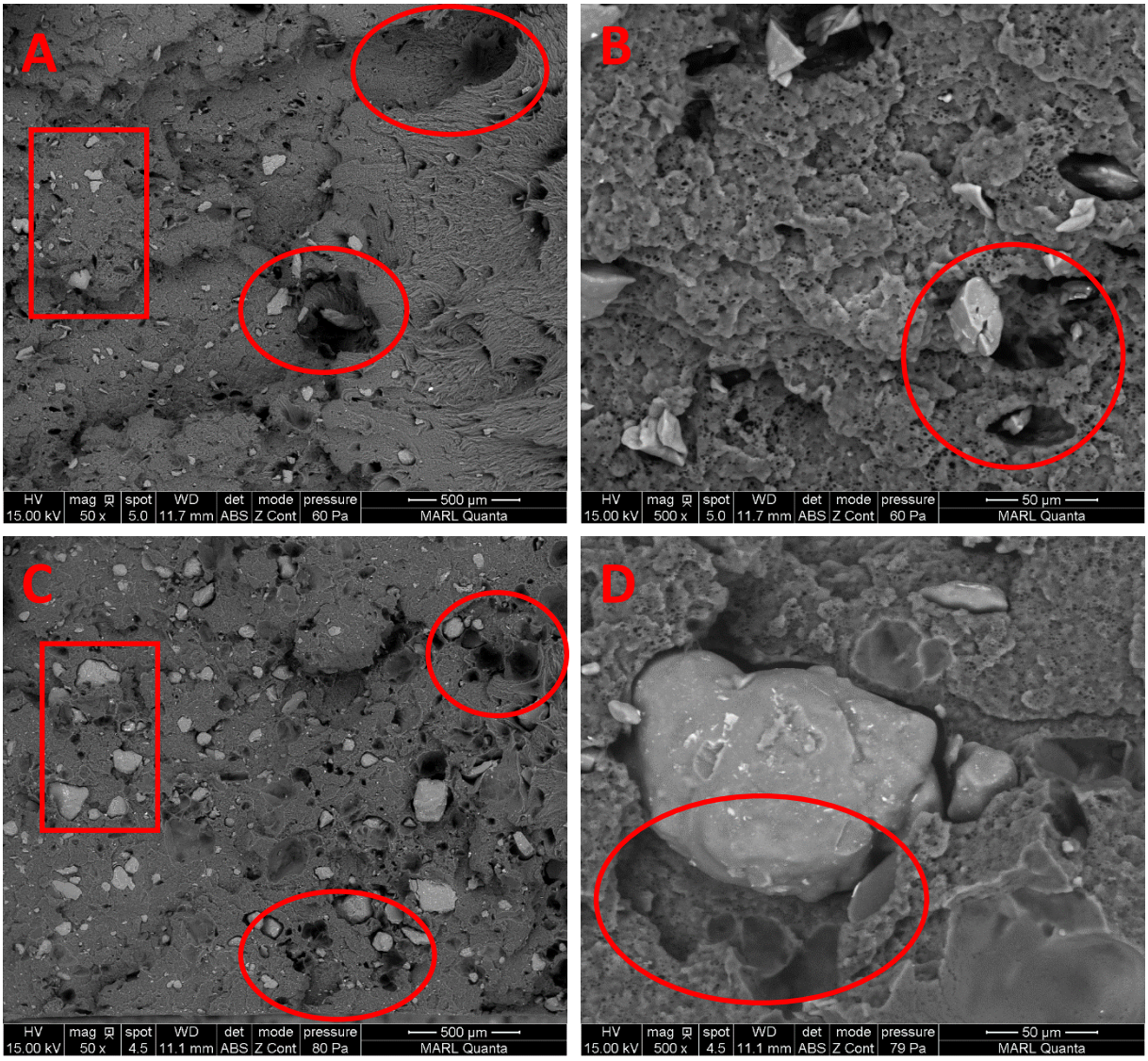

Figure 3.2 *SEM of tensile specimen fracture surface of PP-HPL-MA 94/5/1 single extrusion at 50x magnification (a) and 500x magnification (b); PP-HPL-MA 78/20/2 single extrusion at 50x magnification (c) and 500x magnification (d).*

Physical properties

Specific strength and specific stiffness were calculated as the ratio of ultimate tensile strength to density and Young's modulus to density, respectively. Statistical results for matrix material formulations are presented in tables referred to as "connecting letters tables". These tables consist of sets of letters (population sets) assigned to formulations

based on their statistical difference from other formulations of the same matrix polymer. In more detail, formulations were assigned the same letter if there was no statistical difference when compared to other formulations assigned the same letter. Formulations assigned multiple letters correspond to multiple population sets. Statistical analysis was not performed on MA composites as the MA had little effects in enhancing the ultimate tensile strength.

For LLDPE TPCs, in general the strength was independent of the addition of HPL at levels between 0 and 20% with the exception of 10%. Above 20% HPL filler content, an inversely proportional relationship was observed in ultimate strength. However, at 10% filler content a statistically significant overall increase in strength was observed with the LLDPE-HPL 90/10. A second extrusion cycle resulted in a 22.5% increase in ultimate strength and a 22.1% increase in specific strength when compared to the LLDPE 100 control group, as seen Table 3.4, Figure 3.4, and Figure 3.5. The Young's modulus is generally proportional to the HPL filler level for TPCs as seen in Table 3.4 and Figure 3.3. As seen in Figure 3.5, there was a general increase in specific stiffness at 10% HPL content. Thus, overall for LLDPE, 10% of HPL was the optimum level of filler in terms of strength and stiffness of the TPC. It is believed that addition of HPL generally improves the mechanical properties of the TPC; however, with excessive filler levels (+10%), the HPL tends to agglomerate, reducing the strength of the TPC.

Table 3.4 *LLDPE statistical analysis, displayed in MPa; ultimate strength (left), Young's modulus (right).*

Level of HPL				*Ultimate Strength Mean*		*Level of HPL*				*Young's Modulus Mean*
10	A			11.05773		40	A			439.924
20		B		9.96936		30		B		297.600
5		B		9.76480		20			C	239.265
15		B	C	9.50588		15			D	199.623
0		B	C	9.42280		10			D	198.673
30			C	9.17375		5				E 153.358
40				D 7.36274		0				E 140.305

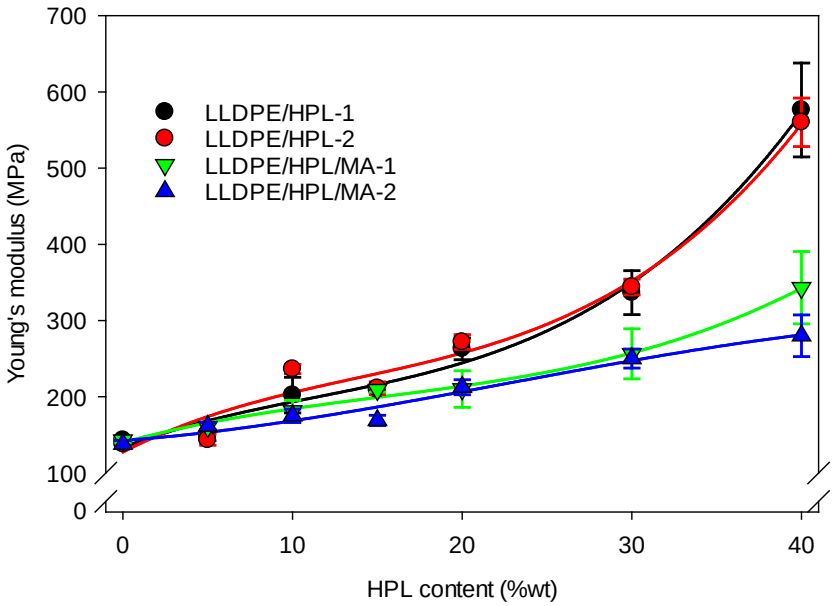

Figure 3.3 *LLDPE TPCs Young's modulus as a function of HPL content.*

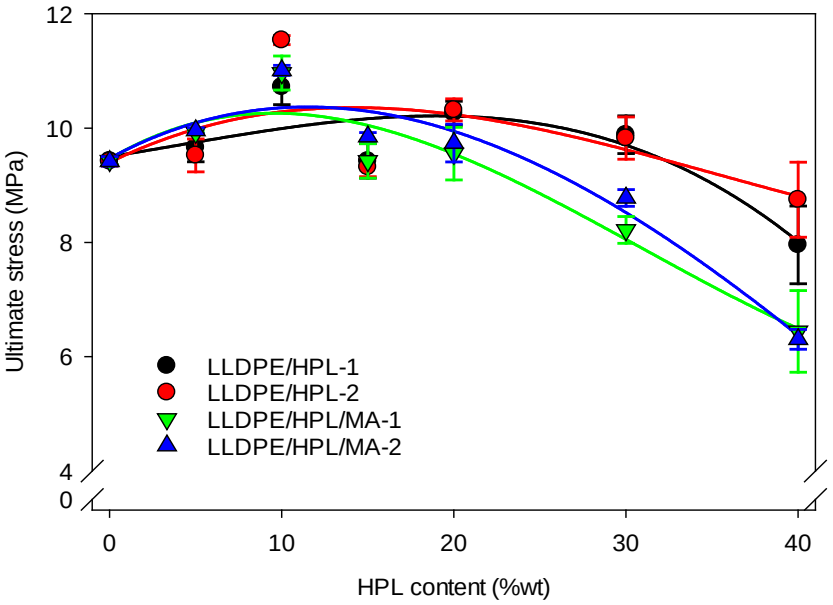

Figure 3.4 *LLDPE ultimate tensile strength as a function of HPL content*

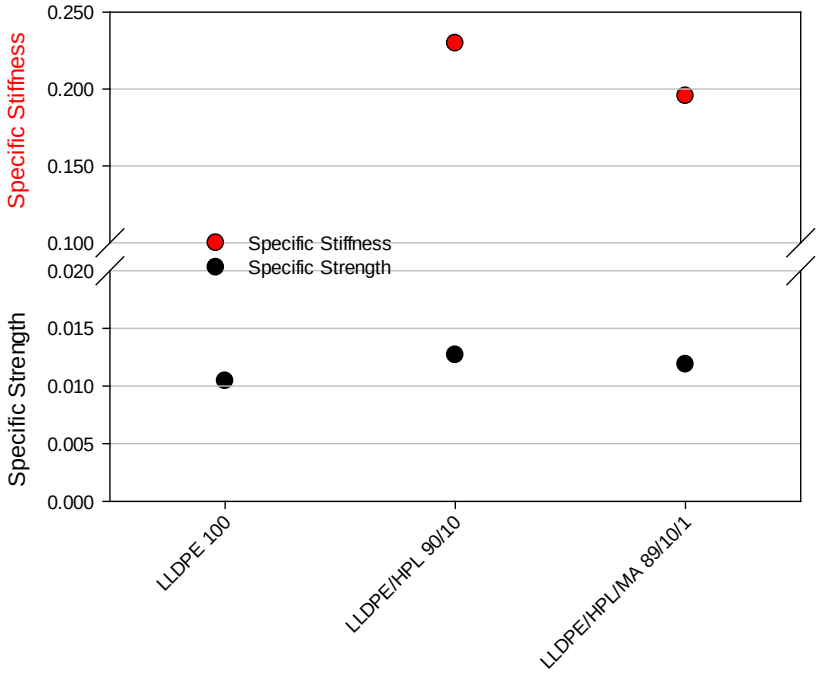

Figure 3.5 *LLDPE single extrusion TPCs specific strength and stiffness for various formulations*

For HDPE TPCs, in general the strength was proportional to the addition of HPL at levels between 0 and 10%. A statistically significant difference in strength at 10% HPL was seen with a 6.7% increase in strength when compared to the control group as seen in Table 3.5. However, above 10% the strength appeared to be inversely proportional to the HPL level, as seen in Table 3.5 and Figure 3.7. It is believed that the higher levels of HPL promoted the generation of stress concentration points because of the limited HPL/matrix interfacial bonding, which became significant above 30% HPL levels. In general, the Young's modulus was proportional to HPL content with a maximum increase of 226% increase with the addition of 40% HPL as seen in Table 3.5 and Figure 3.6. The specific stiffness was increased at 10% HPL, with HDPE-HPL 90/10 exhibiting a 29% increase, shown in Figure 3.8.

Table 3.5 *HDPE statistical analysis, displayed in MPa; ultimate strength (left), Young's modulus (right).*

Level of HPL			*Ultimate Strength Mean*		*Level of HPL*				*Young's Modulus Mean*
10	A		18.3735		30	A			714.855
5	A	B	17.6882		20		B		584.045
0	A	B	17.2106		10			C	499.285
20	A	B	16.4192		15			C	481.9
15	A	B	16.0552		5			D	412.085
30		B	13.5825		0			D	400.1026

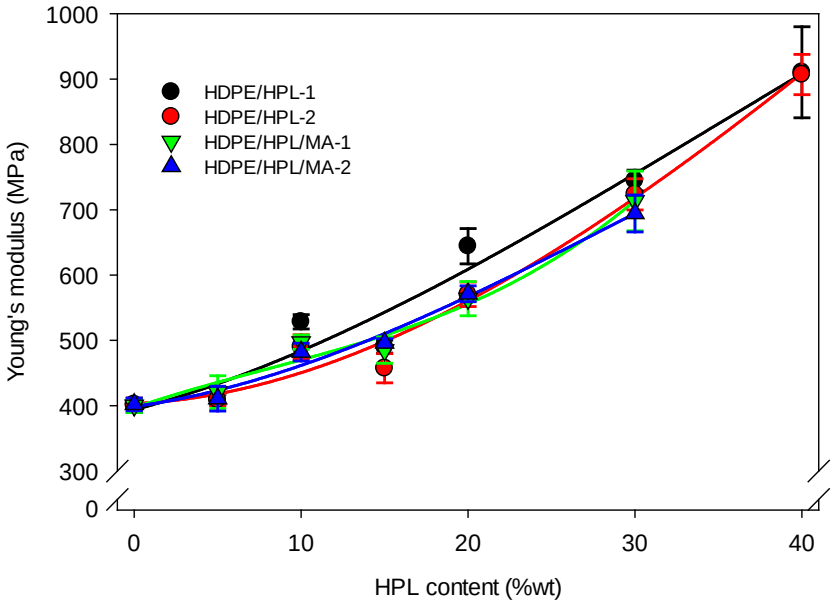

Figure 3.6 *HDPE TPCs Young's modulus as a function of HPL content*

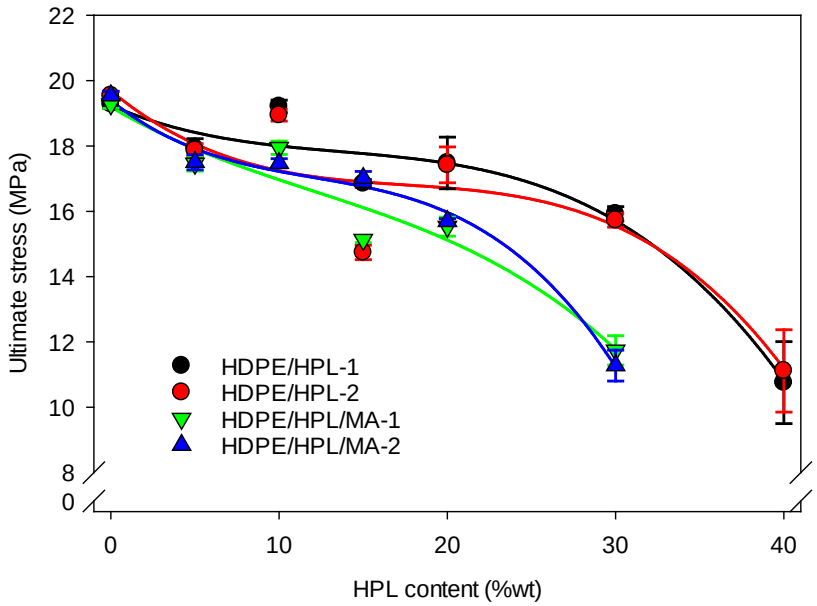

Figure 3.7 *HDPE TPCs ultimate tensile strength as a function of HPL content*

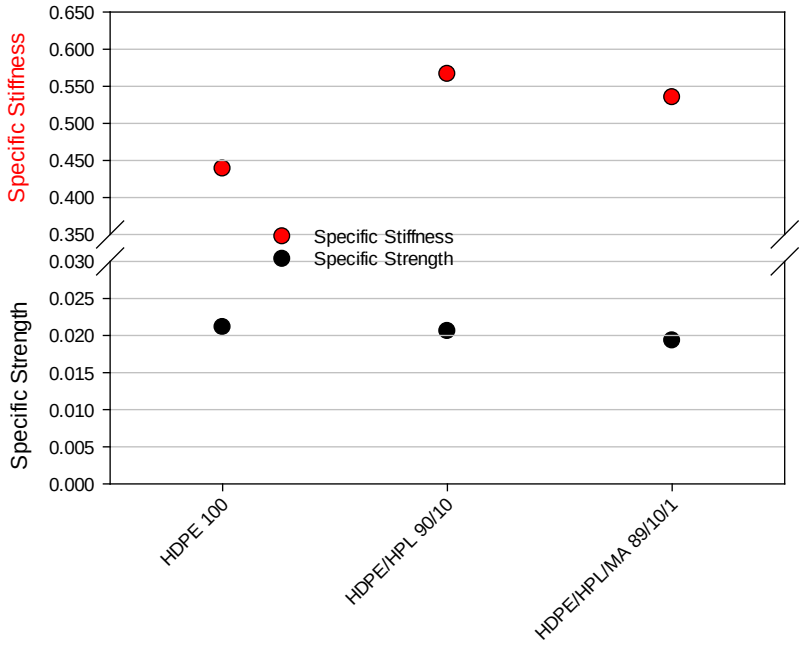

Figure 3.8 *HDPE single extrusion TPCs specific strength and stiffness for various formulations.*

In reference to PP TPCs, in general the strength was inversely proportional to the addition of HPL, as seen in and Figure 3.10. Overall, the Young's modulus of PP TPCs had a proportional relationship with the HPL content, as shown in and Figure 3.9. However, as seen in Figure 3.10, with the PP-HPL-MA 84/15/1 single extrusion material, and the twice extruded PP-HPL 95/5, the TPCs exhibited no loss in ultimate strength when compared to the control group. From Figure 3.11, the specific strength of PP-HPL 90/10 showed no statistical difference from the control. The specific stiffness showed an increase of 31.5% and 27.5% for PP-HPL-MA 89/10/1 and PP-HPL 90/10, respectively when compared to the control group.

Table 3.6 *PP statistical analysis, displayed in MPa; ultimate strength (left), Young's modulus (right).*

Level of HPL		*Ultimate Strength Mean*	*Level of HPL*		*Young's Modulus Mean*
5	A	21.805	20	A	730.602
0	A	21.396	15	A	730.590
10	B	20.477	10	B	686.900
15	C	19.648	5	C	655.485
20	D	17.720	0	D	543.243

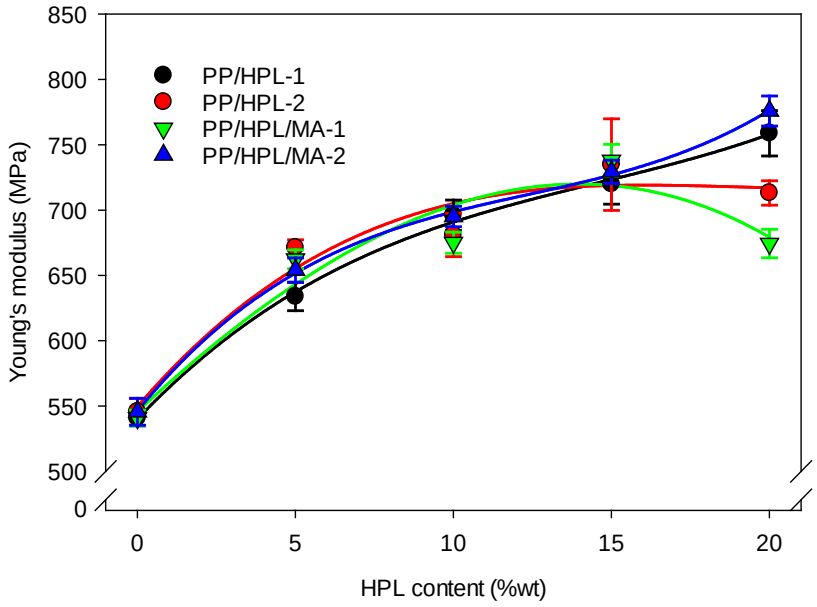

Figure 3.9 *PP TPCs Young's modulus as a function of HPL content*

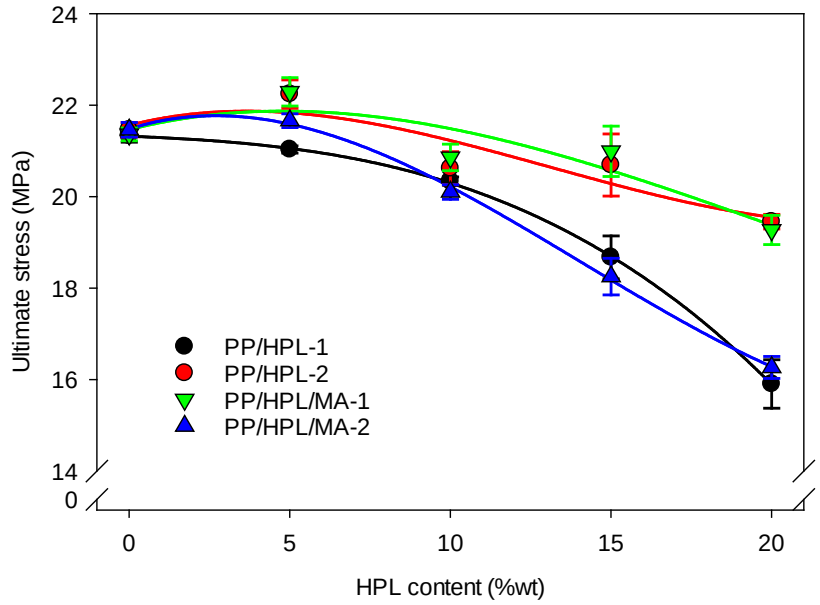

Figure 3.10 *PP TPCs ultimate tensile strength as a function of HPL content*

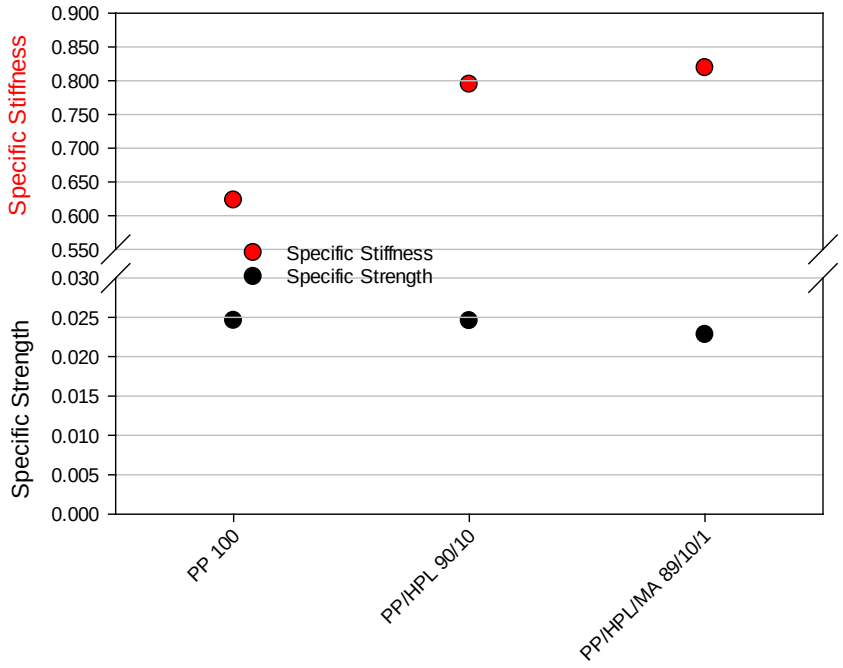

Figure 3.11 *PP single extrusion TPCs specific strength and stiffness for various formulations*

In reference to PPr TPCs, in general the strength was inversely proportional to the addition of HPL, as seen in Table 3.7 and Figure 3.13. It is believed that the higher levels of the HPL promoted the generation of stress concentration points because of the limited HPL/matrix interfacial bonding, which became significant above 15% HPL levels. As seen in Table 3.7 and Figure 3.12, the Young's modulus was generally proportional to the HPL filler level for TPCs, independent of MA compatibilizer treatment. Figure 3.14 shows that the specific strength of PPr-HPL 90/10 was not statistically different, while the specific stiffness increased by 14.6% when compared to the control group. However, at 10% HPL content with MA, specific strength decreased by 22% without statistically significant increase in specific stiffness.

Table 3.7 *PPr statistical analysis, displayed in MPa; ultimate strength (left), Young's modulus (right).*

Level of HPL		*Ultimate Strength Mean*	*Level of HPL*		*Young's Modulus Mean*
0	A	27.045	15	A	759.910
5	B	25.743	10	A	747.083
10	C	24.122	5	B	726.305
15	D	20.334	0	C	692.455

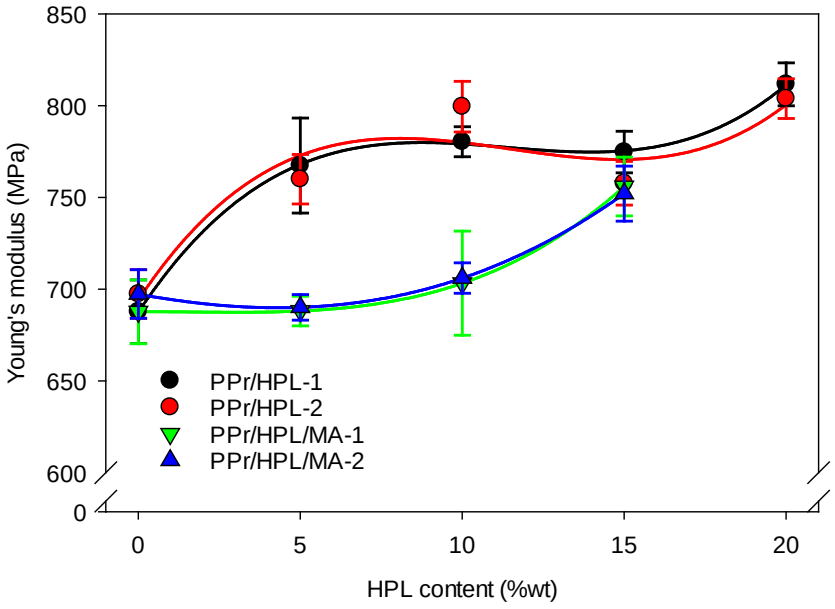

Figure 3.12 *PPr TPCs Young's modulus as a function of HPL content*

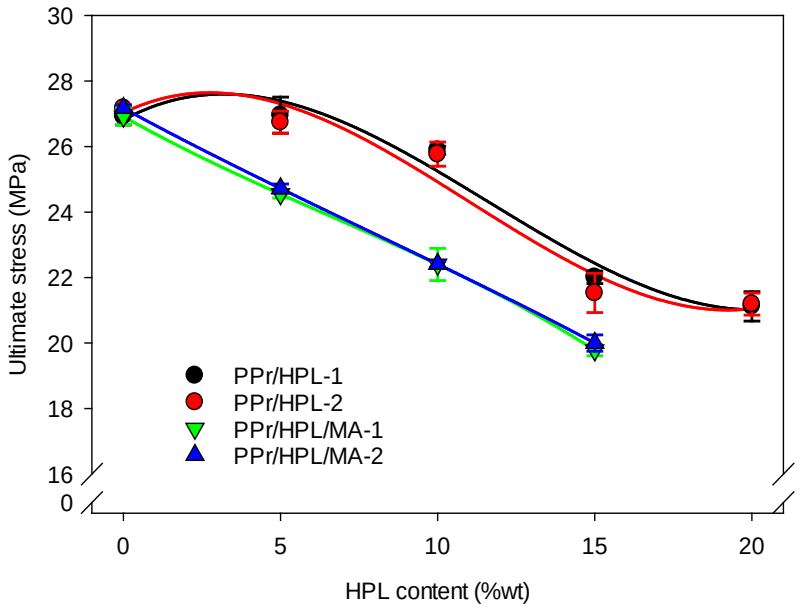

Figure 3.13 *PPr TPCs ultimate tensile strength as a function of HPL content*

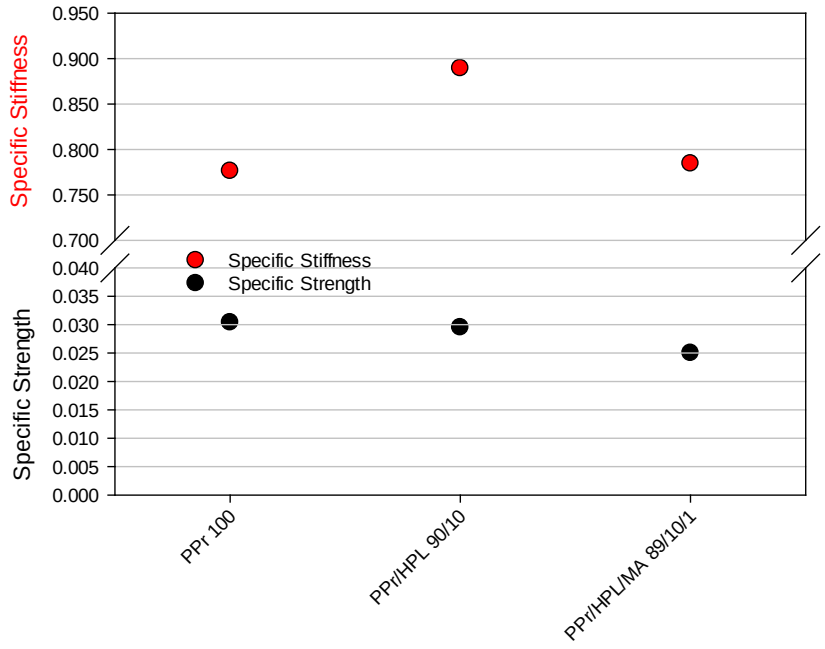

Figure 3.14 *PPr single extrusion TPCs specific strength and stiffness for various formulations*

Conclusions and Recommendations

The results obtained during this study indicate that HPL biocomposites can be a viable alternative to currently available bulk composites used by industry. All HPL biocomposites showed increased stiffness proportional to increased HPL content. LLDPE and HDPE HPL biocomposites showed statistically significant difference in ultimate tensile strength which increased by 22.5% and 6.7%, respectively, at 10 %wt of HPL, proving they have positive effects on mechanical properties compared to the negative control groups of base LLDPE and HDPE.

In addition, PP and PPr HPL biocomposites showed an overall negative impact on ultimate tensile strength with the addition of HPL. It is believed that this decrease in strength can be attributed to the higher processing temperatures of PPs in comparison to

PEs. A secondary cause of diminished strengths may because of the extrusion compounding technique utilized. During extrusion MA and HPL compounded simultaneously forming aggregates within polymer melt and on the extruder screws.

MA, when used as a compatibilizer, showed an overall negative impact on mechanical properties when compared against HPL biocomposites without MA. SEM images showed that the MA increased aggregation of HPL particles and increased voids. Future studies should include the compounding of HPL onto MA grafted PPs and PEs. I believe aggregates concentrations would greatly diminish and overall increased wetting interactions at interfaces.

Secondary extrusion showed to have an overall negligible effect on the mechanical properties of HPL biocomposites, independent of polymer matrix, HPL content, and MA. Future testing could provide insight regarding the thermal effects of higher processing temperatures, such as experienced with PP, on ultimate tensile strength. Any future investigation should also include a techno-economic analysis (TEA) on the production of HPL biocomposites to assess the cost competitiveness against current materials used by industry.

CHAPTER 4. AGAVE FIBER THERMOPLASTIC COMPOSITES

Journal article for presentation to the Journal of Polymer Science

Mitchel Michel[a], Alper Kiziltas[b], Richard Hoch[c], Yucheng Peng[d], David Grewell[a], Reza Montazami[e],

[a] Agricultural and Biosystems Engineering, Iowa State University, Ames, IA 50011, USA

[b] Ford Motor Company, Dearborn, MI 48120, USA

[c] Diageo, London, NW10 7HQ, UK

[d] Berry Plastics, Des Moines, IA 50321, USA

[e] Department of Mechanical Engineering, Iowa State University, Ames, IA 50011, USA

Objectives

The objectives of this study were to:

1. Develop a low-cost, biobased agave fiber composite to serve as a "one-to-one drop-in" for traditional plastics and/or composites.
2. Determine the viability of developing agave fiber as a filler for PP, LLDPE, and HDPE matrix polymers.
3. Develop agave-based composite formulations that have enhanced mechanical properties, namely tensile strength, impact strength, elongation, and stiffness.
4. Utilize a compatibilizer to improve filler-matrix bonding of agave-based composites.
5. Develop a low-cost and scalable approach to process agave bagasse to isolate fibers.

6. Develop a low-cost and scalable approach to control and eliminate the odor of agave fiber-polypropylene (AF-PP) composites.
7. Develop extrusion and injection molding processing conditions and parameters for properly producing agave-based composite components/products.
8. Characterize the mechanical properties, performance, and density of agave-based composites.
9. Characterize filler-matrix bonding using scanning electron microscopy.
10. Develop design recommendations for producing agave fiber-based composite products/components.

Introduction

The blue agave plant is cultivated for the production of tequila, an alcoholic beverage consumed worldwide. The manufacturing and distillation utilizes the core (pina) of the agave plant. Harvested pinas are kilned, crushed, and diluted into water solutions to extract sucrose and fructose for fermentation and distillation of tequila. Agave bagasse is a resulting coproduct that is currently being underutilized, used only for burning as energy or even landfilled. Within the agave bagasse are sisal fibers that have mechanical properties (tensile strength of 183 MPa, and stiffness of 15 GPa) competitive to synthetic fibers such as e-glass (tensile strength of 201 MPa, and stiffness of 13 GPa) [5]. A major disadvantage of these fibers is their hydrophilicity when compounding with hydrophobicity plastics, leading to poor interfacial bonding without pretreatment or compatibilizer.

Materials utilized by industry must meet the engineering requirements of the target application while remaining cost effective. As value-added pretreatments and compatibilizer incorporation are used to pretreated, the resulting composites can exhibit

higher mechanical properties. A potential negative consequence of pretreatment is increased unit cost ($/lb). In order to achieve cost competitiveness with current market materials, a low-cost and scalable approach for producing these biocomposite materials must be achieved.

In this study, the compounding of commodity thermoplastic polymers (PP, LLDPE, and HDPE) with agave fibers through thermal extrusion was achieved. These biocomposites, absent a compatibilizer, are designed to be low-cost alternatives. Additionally, a PP / agave fiber biocomposite was compounded with maleic anhydride (MA) as a compatibilizer. The thermomechanical effects of this value added biocomposite were then compared with biocomposites without MA.

Experimental

Materials

The thermoplastic matrix materials used in this study include a high-density polyethylene (HDPE), linear low-density polyethylene (LLDPE), polypropylene (PP), and polypropylene-r (PPr). The HDPE had a melt flow index of 20 g/10 min at 190 °C and a density of 0.952 g/cm3 (Chevron Phillips Chemical Company LP, Texas). The LLDPE had a melt flow index of 20 g/10 min at 190 °C and a density of 0.925 g/cm3 (ExxonMobil Chemical Corporation, Texas). The PP had a melt flow index of 20 g/10 min at 230 °C and a density of 0.868 g/cm3 (Formosa Plastics 87Corporation, Texas). The polypropylene (PPr) had a melt flow index of 34 g/10 min at 230 °C and a density of 0.91 g/cm3 (Asahi Kasei Plastics Corporation, Michigan).

The agave fibers (AF) used in this study were of the species agave tequilana and were supplied by two sources, Byogy Renewables Inc. provided agave fibers (AF-B) and

Don Julio (Jalisco, Mexico), a manufacturing company within Diageo Corporation, provided agave fibers (AF-D) in blue agave bagasse form. Compatibilizer agent maleic anhydride (MA) had a molecular weight of 98.06 g/mol (Sigma-Aldrich).

Sample preparation

Initially, AF-D bagasse must be separated into heterogeneous fibers of varying lengths and the pith, a non-fibrous spongy organic material in the form of fine particles [11]. This separation included hammer milling to separate the fiber-fiber entanglements. During the milling cycle, bagasse was filtered through screens which isolated fibers from cellulosic and mineral contaminants as seen in Figure 4.1. A total of three 1-minute hammer milling iterations was repeated through (1.5875 mm), (1.5875 mm), and (3.175 mm) screens respectively accomplished both functions. Milled fibers were then placed into a container and tossed. This allowed for further separation of mineral contaminants of higher densities than the fibers to settle at the bottom of the container. Fluffed fibers were removed from the upper portion of biomass/contamination mixture. This process was continued until contaminants were no longer visible within fibers at the bottom of the containers after being fluffed.

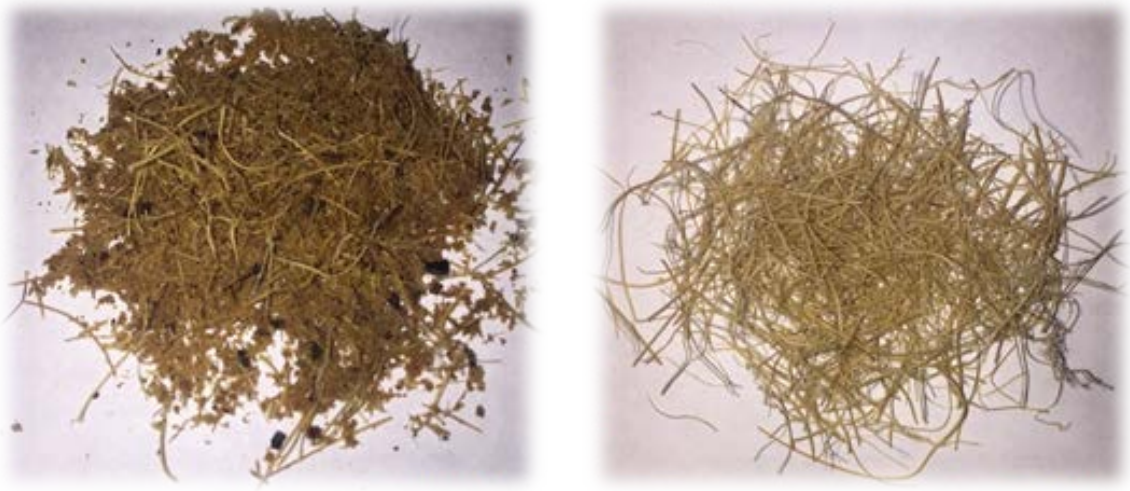

Figure 4.1 *AF-D as received in its raw form containing cellulosic and mineral contaminants (left), isolated fibers post milling process (right).*

Subsequently, AF-B and AF-D underwent a wash treatment to remove dissolvable fractions, mainly residual sugars [12]. In more detail, the fibers were suspended in a water solution at an agave fiber concentration of 20%. The solution was added to a Feldmeier 70-liter jacketed tank and stir-agitated with a Lightnin prop-type variable speed mixer (see Figure 4.2). A Chromalox microtherm CMX-250-240 regulated the jacket's temperature at 70 °C to heat the solution for 24 h. Upon completion of the AF-B cycles, a waste water sample was collected. Between cycles, fibers were strained from solution with no. 30 mesh (US Standard Sieve Series, Dual MFG Corporation, Chicago Illinois, USA). This process was then repeated for a total of seven wash cycles for AF-B and three wash cycles for AF-D as three cycles showed to eliminate 95% of dissolvable carbohydrates from wash trials conducted on AF-B.

Figure 4.2 *Photograph of Feldmeier 70-liter jacketed tank*

Washed fibers were spread onto drying trays at a thickness of <50 mm and dried at 105 °C for 18-24 h in a Humboldt H-30135 convection oven. Once dried, AF-D fibers were cut to lengths of <12 mm with an Ingento paper cutter.

Co-extrusion of agave fiber with thermoplastics

Matrix polymers LLDPE, HDPE, and PP were melt blended with AF-B and PP-r with AF-D in a Leistritz 18-mm co-rotating twin-screw extruder with a barrel – l/d ratio of 25:1. The temperature profiles (°C) and extrusion speeds (RPM) used for the compounding are detailed in Table 4.1.

Table 4.1 *Thermal extrusion temperature profiles (°C) and speed parameter (RPM).*

Heating Zones		*1 (hopper)*	*2*	*3*	*4*	*5*	*6*	*Screw Speed (RPM)*
Resin	LLDPE	165	175	180	175	170	165	250
	HDPE	175	180	185	185	180	170	225
	PP	190	210	215	215	200	190	170
	PP-r	195	210	215	220	215	210	275

Materials were fed into the extruder using a Schenck AccuRate volumetric feeder with speeds of 100-200 RPM. Materials were premixed and fed simultaneously into extruder zone 0. The formulations compounded are detailed in Table 4.3 and Table 4.2.

Table 4.2 *Formulation details of PPr AF-D formulations.*

Base Resin	*% Resin*	*% Filler*	*% Treated Filler*	*% Maleic Anhydride*
PPr	100	0	0	0
	90	10	0	0
	80	20	0	0
	70	30	0	0
	60	40	0	0
	90	0	10	0
	80	0	20	0
	70	0	30	0
	60	0	40	0
	99	0	0	1
	89	0	10	1
	79	0	20	1
	69	0	30	1
	59	0	40	1

Table 4.3 *Formulation details of LLDPE, HDPE, and PP AF-B formulations.*

Base Resin	*% Resin*	*% Filler*
HDPE	100	0
	95	5
	90	10
	85	15
	80	20
	70	30
	60	40
PP	100	0
	95	5
	90	10
	85	15
	80	20
	70	30
	60	40
LLDPE	100	0
	95	5
	90	10
	85	15
	80	20
	70	30
	60	40

Injection molding of test specimens

A BOY 22S, 28-mm injection molding machine was used to mold tensile test specimens from the various formulations. The temperature profiles utilized are detailed in Table 4.4.

Table 4.4 *Thermal injection molding temperature profiles (°C) of thermoplastic AF-B and AF-D composites.*

Heating Zone		*1 (hopper)*	*2*	*3*	Mold Temp
Resin	LLDPE	175	180	170	45
	HDPE	180	185	175	52
	PP	190	210	190	52
	PP-r	190	210	190	52

Morphology

Scanning electron microscope (SEM) images were taken of tensile test fracture surfaces to characterize the effects of the maleic anhydride as a compatibilizer. Sample fracture surfaces were not sputter coated prior to SEM preparation as this was only for qualitative analysis, and only relatively low magnifications were used in an environmental SEM. This also allowed back scatter characterization of the chemical composition of the surfaces.

Tensile test

Tensile tests were conducted according to ASTM D638-14 [10] for Type I specimens with a testing speed of 50 mm/min. The ultimate tensile strength, 0.2% yielding strength, Young's modulus, and percent elongation at peak stress were calculated from a constant cross head displacement for 10 specimens within each sample group. Cross sectional area of specimens was calculated with a Fowler electronic caliper prior to test and assumed constant throughout testing. This assumption was then used to determine the percent elongation absent an extension meter.

Density test

The average densities of the composites were determined from dry initial weights and immersion of thermally compounded pelletized samples. Dry convection oven sample weights were measured and recorded. Samples were then submerged into 2-propanol and volumetric displacement measured within a graduated cylinder. The average density was calculated as defined in Equation 18, where (ρ_c) is the composite density, (m) is the dry mass of the composite sample, (V_i) is the initial volume, and (V_f) is the final volume measured within the graduated cylinder after composite was inserted.

$$\rho_c = \frac{m}{V_f - V_i}$$

Equation 18

Carbohydrate concentration

Carbohydrate (CHO) concentration of agave fibers was calculated from the seven collected waste water samples of post wash treatments of AF-B. Samples were tested twice and CHO concentrations were quantified using a phenol-sulfuric acid colorimetric method [13]. To obtain the control curve, control samples of four known glucose concentrations were prepared and tested at A490 on a Thermo Fisher Genesys 30; the visible spectrophotometer results are shown in Table 4.5.

Table 4.5 *Glucose analysis control concentrations and light absorbance.*

µL	*Glucose Concentration (**µG**)*	*A490 absorbance*
0	0	0
5	5	0.117
20	20	0.45
40	40	0.925
80	80	1.74

Odor analysis

Odor analysis of PP-r / AF-B composites was performed to determine the viability of AF thermoplastic composites for consumer acceptance. Tests were performed in accordance to a modified standard of Ford Motor Company laboratory test method BO 131-03 [14] variant A. Tests utilized four formulations detailed below in Table 4.6.

Table 4.6 *Formulations utilized for odor analysis.*

Base Resin	*% Resin*	*% Filler*	*% Treated Filler*	*% Maleic Anhydride*
PPr	100	0	0	0
	70	30	0	0
	70	0	30	0
	69	0	30	1

The standard's variant A, which is designed for the testing of molded car parts, was modified to incorporate injection molded tensile specimens. Apparatuses used were 3-liter odorless preserving jars with a polyethylene closed cell foam, 3 mm thick of 45 kg/m^3 density. 50 mL of water was added and one specimen was suspended in the jar

with a binder clip as shown in Figure 4.3. Sealed jars were tested under the conditions detailed in Table 4.7 within a Humboldt H-30135 convection oven.

Figure 4.3 *Photograph of odor test sample of 3 Liter jar containing molded specimen*

Table 4.7 *Summary of odor test conditions.*

Condition	*Temperature*	*Test Time*
1	23 ± 2 ºC	24 h ± 1 h
2	40 ± 2 ºC	24 h ± 1 h
3	65 ± 2 ºC	2 h ± 10 min

Odor analysis was performed by five panelists that consisted of two male and three female subjects ages 19 to 27 years. A female majority was preferred as women's olfactory sensitivity increases faster and to a greater degree compared to males [15]. Panelists evaluated odor according to the rating scale criteria detailed in Table 4.8.

Table 4.8 *Odor rating scale criteria.*

Rating Scale	***Description of Rating***
Rating 1	not perceptible
Rating 1.5	slightly perceptible
Rating 2	perceptible, not disturbing
Rating 2.5	clearly perceptible but not disturbing
Rating 3	very perceptible but not disturbing
Rating 3.5	intense enough to be slightly disturbing
Rating 4	disturbing
Rating 4.5	intense and disturbing
Rating 5	strongly disturbing
Rating 5.5	very intense, disturbing
Rating 6	extremely disturbing

The standard provides the following description of a disturbing odor, “The definition of a disturbing odor is one that would be considered inappropriate for a ‘new car’ smell. The smell of a component/ material is defined as disturbing, not when it is more concentrated, but rather when it transitions from one acceptable odor to another unacceptable odor upon conditioning. The concentrated odor of hot plastic, hot rubber, hot leather, etc. would not qualify as a disturbing odor. A disturbing odor or inappropriate smell is also one that is identifiable as smells that are not normally associated with the interior of a new car, (i.e. sour milk, fish, perfume, burnt, musky, asphalt, rotten meat)” [14].

Thermal stress conditioning

Impact test specimens included virgin PP-r, PP-r/MA at 99/1, PP-r/AF-D washed at 90/10, PP-r/AF-D washed at 90/10, and PP-r/MA/AF-D at 89/1/10. Specimens of each composition were placed in pans and inserted in convection ovens held constant at 120 °C and 140 °C for 1000 h. Test specimen groups contained five replicate samples for each temperature condition. These samples were later characterized for thermal mechanical properties, i.e., impact testing.

Impact test

Charpy impact tests were conducted according to ASTM D6110-10 [16] on injection molded specimens using a Tinus Olsen Model 927 Impact Tester. Impact strengths were measured from the energy lost in broken specimens. The cross sectional area of specimens was calculated with a Fowler electronic caliper prior to test and assumed constant throughout testing.

Results and Discussion

Carbohydrate concentration

The Phenol-H2SO4 method was used to quantify the amount of residual dissolvable sugars and polysaccharides within the agave fibers after fermentation. Based on the control glucose solution tests shown in Figure 4.4, a linear fit regression was performed and resulted in Equation 19. This equation was used to quantify the amount of sugar removed with the individual wash treatments as seen Figure 4.5. From this analysis, a reduction of 95% CHO’s was observed after three wash treatments.

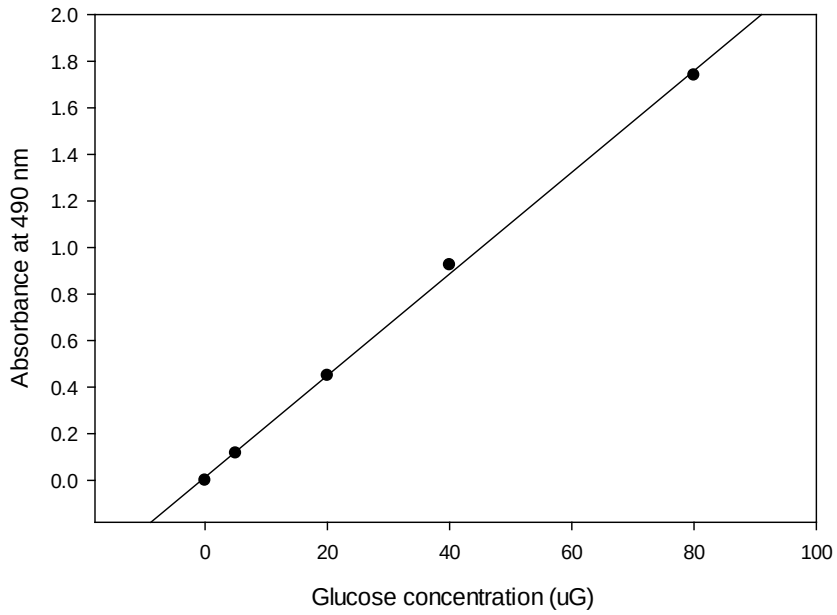

Figure 4.4 *Absorbance as a function of Glucose Concentration Controls with Linear Fit*

$$F(x) = 0.0217x + 0.0229$$

Equation 19

A glucose control concentration Linear Fit Equation where (F(x)) is the absorbance reading at a wavelength angle of A490 from the spectrophotometer and (x) is the predicted glucose concentration.

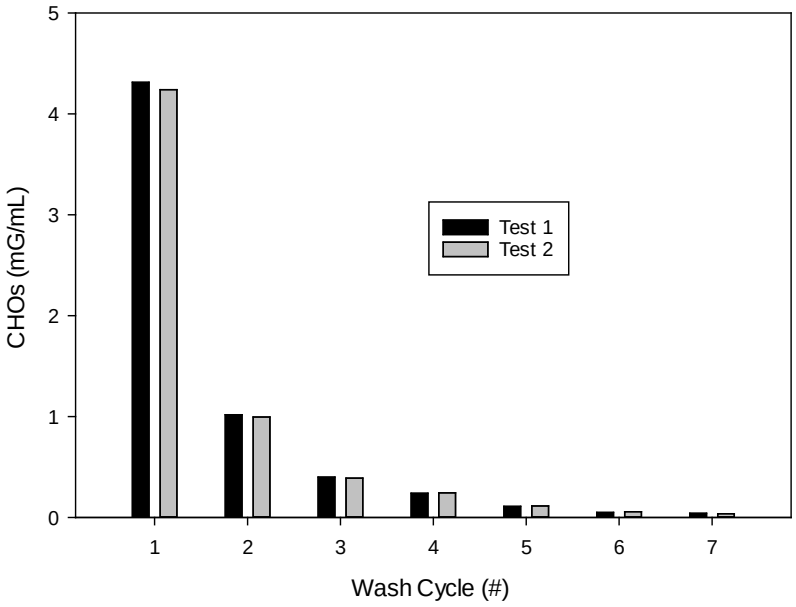

Figure 4.5 *CHO concentrations of post wash treatment water solutions*

Morphology

SEM images of unwashed AF-D show that the fiber surfaces contain residual cellulosic structures within the fibers (seen in Figure 4.6a and Figure 4.6b), as well as mineral particles in and on the surfaces (seen in Figure 4.6c). Voids parallel to the fibers show mineral particles entangled within the cellulosic structures, as seen in Figure 4.6a. In comparison, washed fiber images showed fewer loss/weak dissolvable cellulosic structures with porous surfaces (see Figure 4.7c) and an increased frequency of voids parallel to the fiber (see Figure 4.7a and Figure 4.7b).

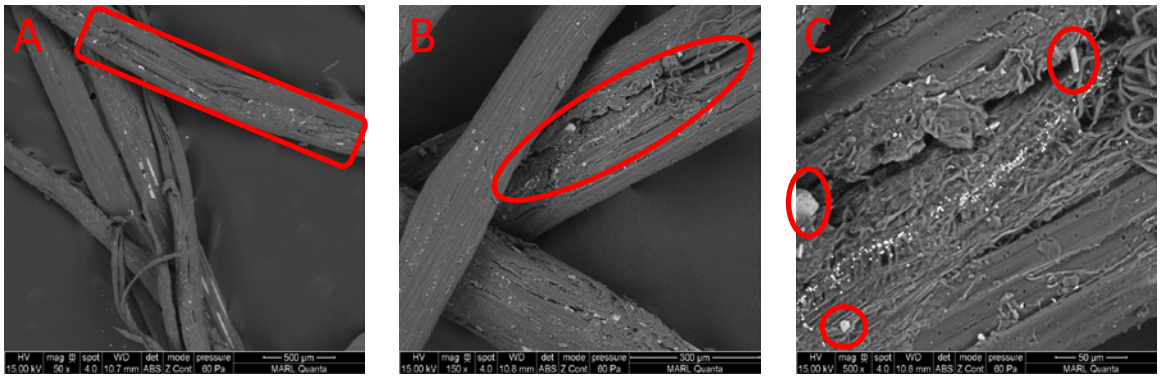

Figure 4.6 *SEM images of unwashed AF-D showing voids parallel to the fibers with mineral particles entangled within the cellulosic structures at 50X magnification (a), at 150X magnification (b), and at 500X magnification (c).*

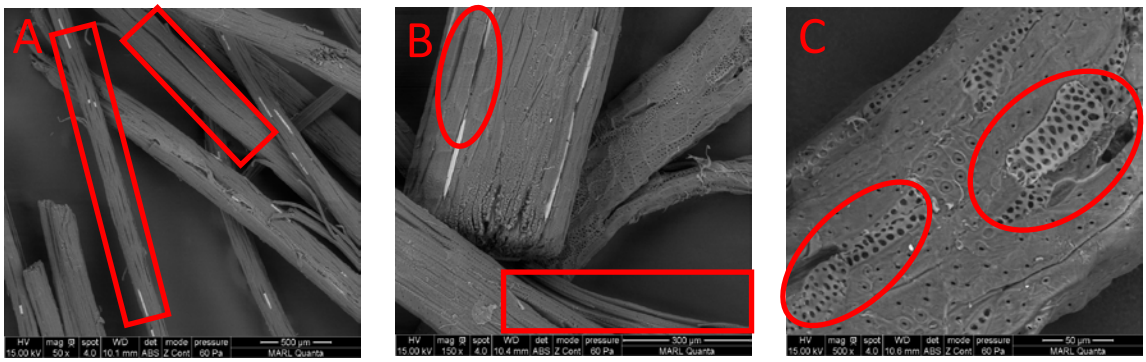

Figure 4.7 *SEM images of washed AF-D showing voids parallel to the fiber at 50x magnification (a) and at 150x magnification (b), porous surface features at 500x magnification (c).*

SEM images were also taken of PPr/AF-D tensile test fracture surfaces to characterize the effects of increased fiber content. As seen in Figure 4.8a, at 10% fiber content, limited regions have fibers entangled (red ovals) upon one another. However, at 30% fiber content it is seen that there is an increased fiber entanglement (red ovals), as seen in Figure 4.8b.

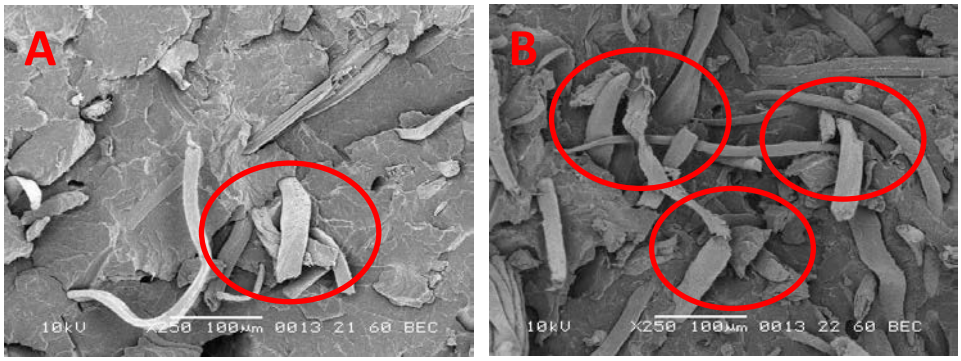

Figure 4.8 *SEM images of fiber entanglement with composite for PP-r/AF-D unwashed at 90/10 %wt at 250x magnification (a) and at 70/30 %wt at 250x magnification (b).*

Odor analysis

The results of odor analysis tests completed using the Ford standard protocol [14] are summarized in Figure 4.9. The results showed a proportional relationship between the odor rating and the level of incorporation of agave fibers. In addition, the ambient temperature at which the test was completed increased the odor rating. It is important to note that using the odor rating scale from Table 4.7, an odor rating of 3 indicates that the odor is very perceptible but not disturbing. Thus, based on these thermal odor tests, it is seen that all of the tested specimens are suitable biocomposite materials with regard to consumer acceptance.

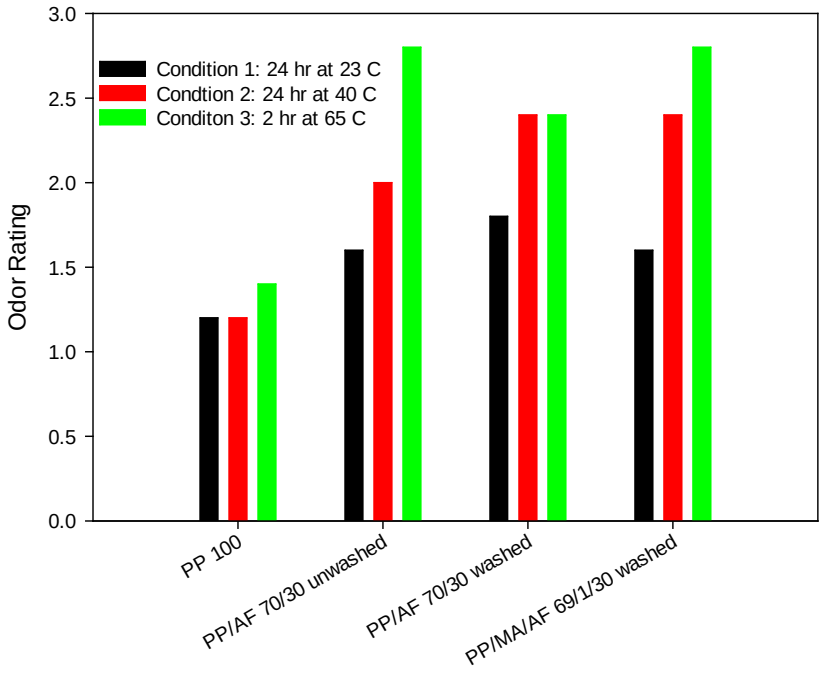

Figure 4.9 *Odor analysis results of PP-r/AF-D heat treatments for various formulations*

Physical properties

In reference to the HDPE/AF-B composites, it is seen (Figure 4.10) that in general the strength is inversely proportional of the addition of AF-B at levels between 0 and 20%. However, above 20% the strength appears to be proportional to the AF-B levels, see Figure 4.10. It is believed that higher levels of AF-B resulted in fiber entanglements and promoted the increase in strength, which became significant above 20% AF-B levels. In addition, in general, the Young's modulus was proportional to AF-B content, with a maximum increase of 231% (compared to no AF-B) with the addition of 40% AF-B, as seen in Figure 4.11. In general, the %elongation was inversely proportional with an initial decrease of 89.5% at 5% AF-B and 97% at 40% AF-B (compared to no AF-B), as seen in Figure 4.12. In

general, the 0.2% yield strength is proportional of the addition of AF-B content with a maximum increase of 36.1% at 40% AF-B (compared to no AF-B), as seen in Figure 4.13.

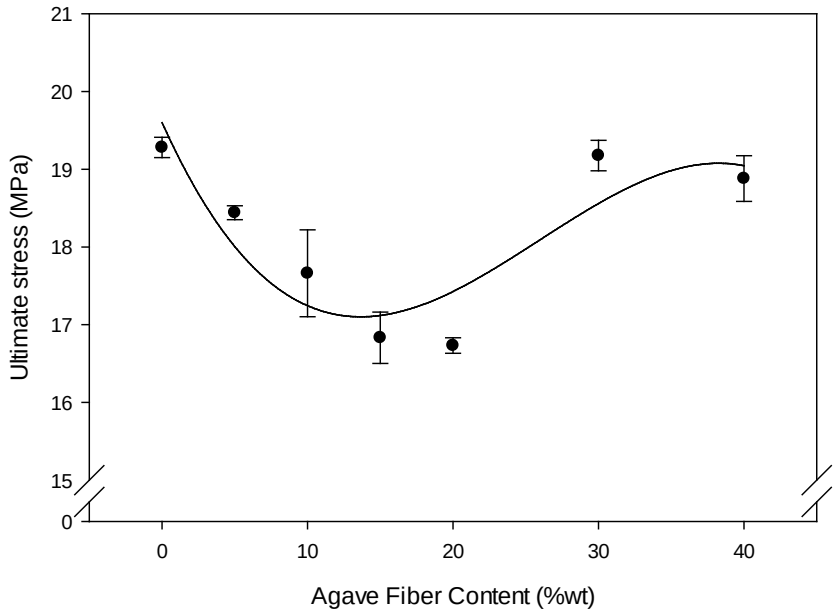

Figure 4.10 *HDPE/AF-B ultimate tensile strength as a function of AF content*

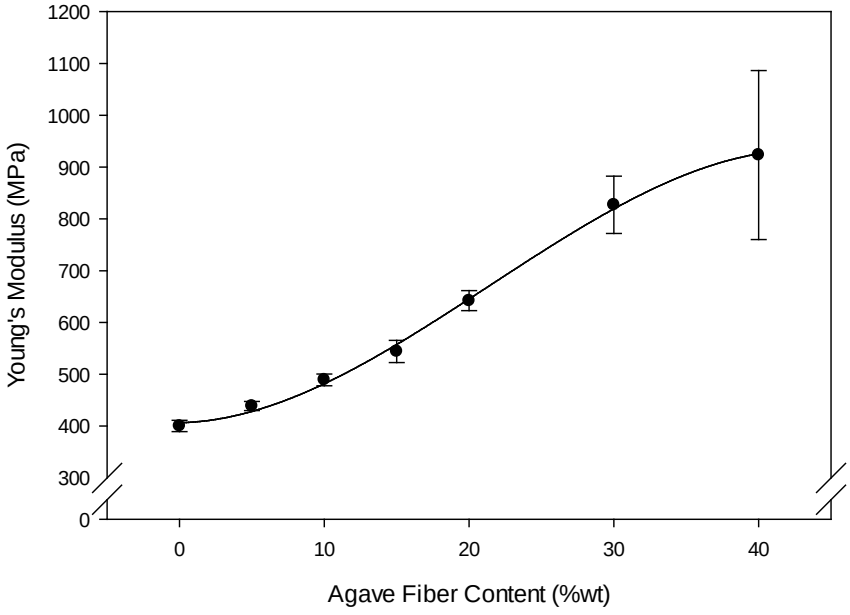

Figure 4.11 *HDPE/AF-B Young's modulus as a function of AF content*

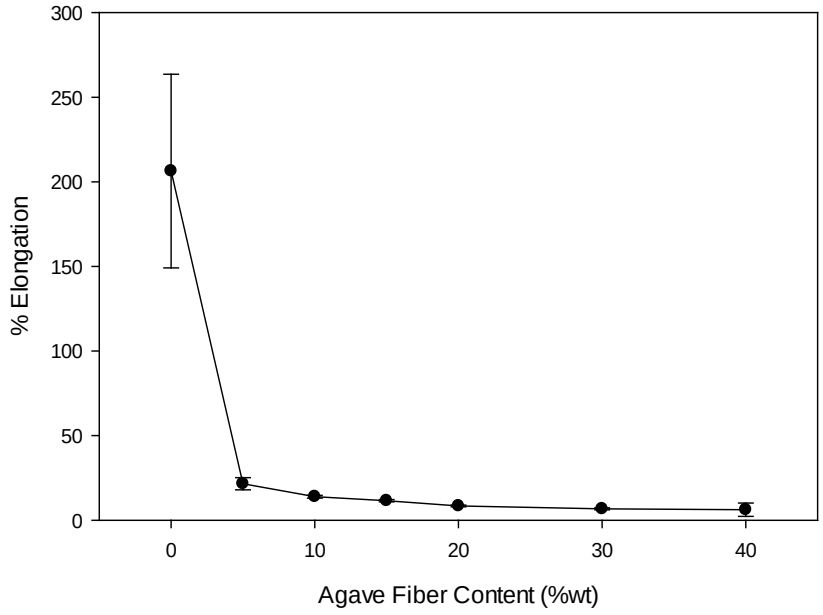

Figure 4.12 *HDPE/AF-B elongation as a function of AF content*

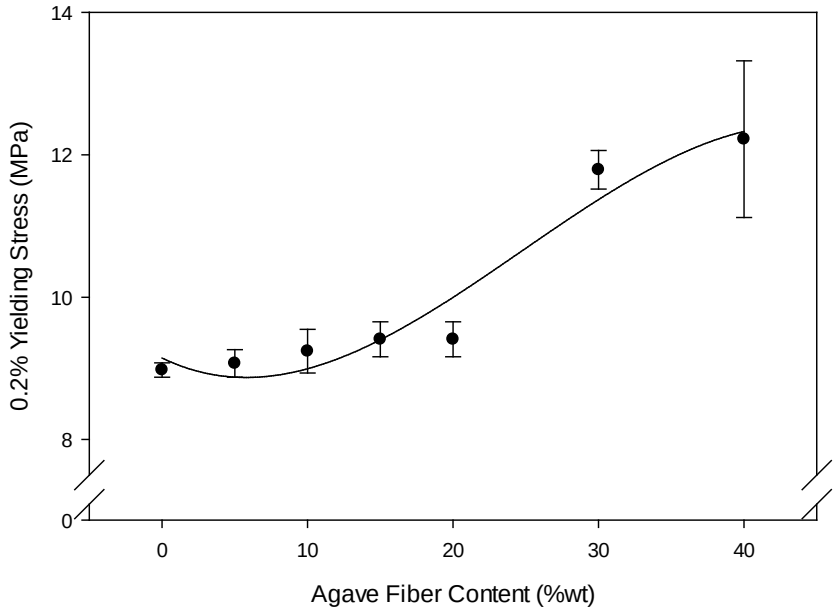

Figure 4.13 *HDPE/AF-B 0.2% yielding stress as a function of AF content*

In reference to LLDPE/AF-B composites, it is seen that in general the strength is proportional of the addition of AF-B with a maximum increase of 150% with the addition

of 40% AF-B as seen in Figure 4.14. In general, the Young's modulus is proportional to AF-B content with a maximum increase of 425% (compared to no AF-B) with the addition of 40% AF-B as seen in Figure 4.15. In general, the %elongation was inversely proportional with an initial decrease of 91.7% at 5% AF-B and 99.1% at 40% AF-B (compared to no AF-B), as seen in Figure 4.16. In general, the 0.2% yield strength is proportional of the addition of AF-B content with a maximum increase of 221% (compared to no AF-B), as seen in Figure 4.17.

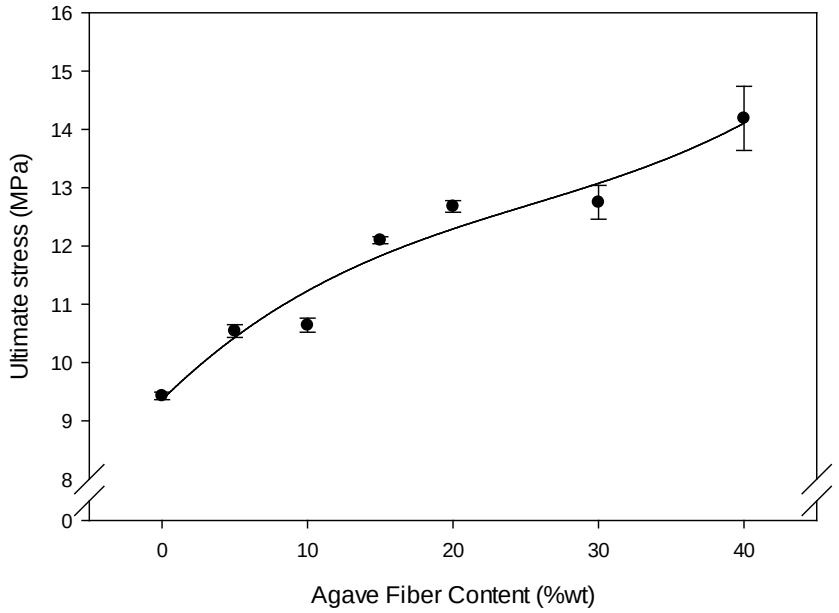

Figure 4.14 *LLDPE/AF-B ultimate tensile strength as a function of AF content*

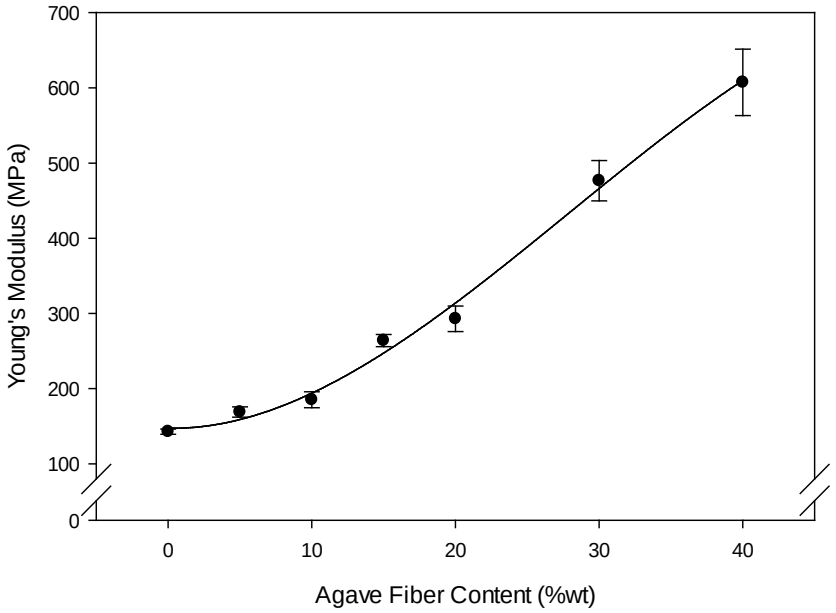

Figure 4.15 *LLDPE/AF-B Young's modulus as a function of AF content*

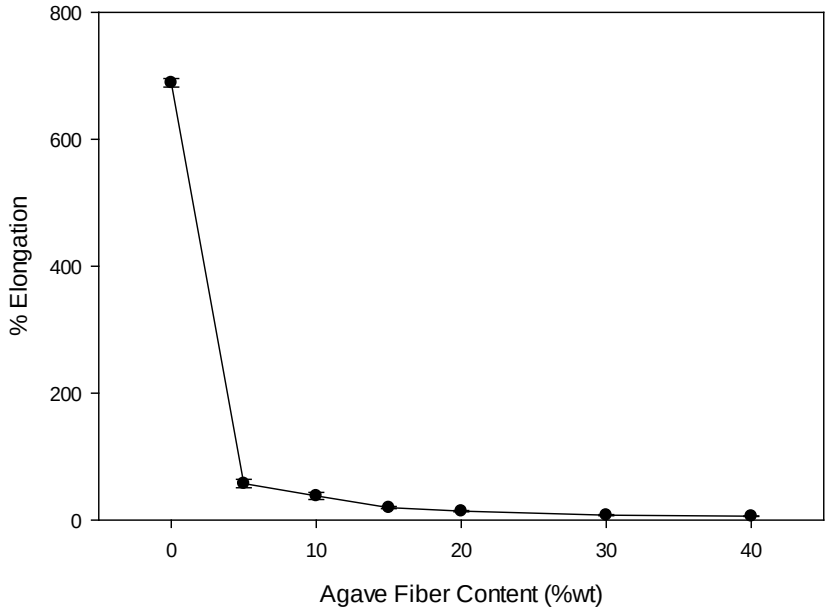

Figure 4.16 *LLDPE/AF-B elongation as a function of AF content*

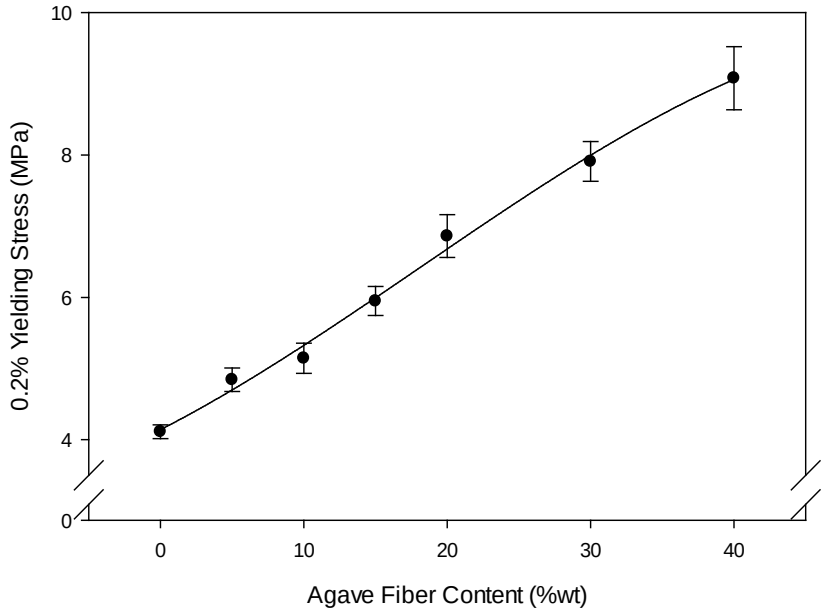

Figure 4.17 *LLDPE/AF-B 0.2% yielding stress as a function of AF content*

In reference to PP/AF-B composites, in general the ultimate strength was independent of the addition of AF-B at levels between 0 and 40% with strengths only ranging from 21.01-22.29 MPa as seen in Figure 4.18. In general, the Young's modulus was proportional to AF-B content, with a maximum increase of 194% (compared to no AF-B) with the addition of 40% AF-B, as seen in Figure 4.19. In general, the %elongation was inversely proportional with an initial decrease of 89.4% at 5% AF-B and 97% at 40% AF-B (compared to no AF-B), as seen in Figure 4.20. In general, the 0.2% yield strength is proportional of the addition of AF-B content with a maximum increase of 20.7% at 40% AF-B (compared to no AF-B), as seen in Figure 4.21.

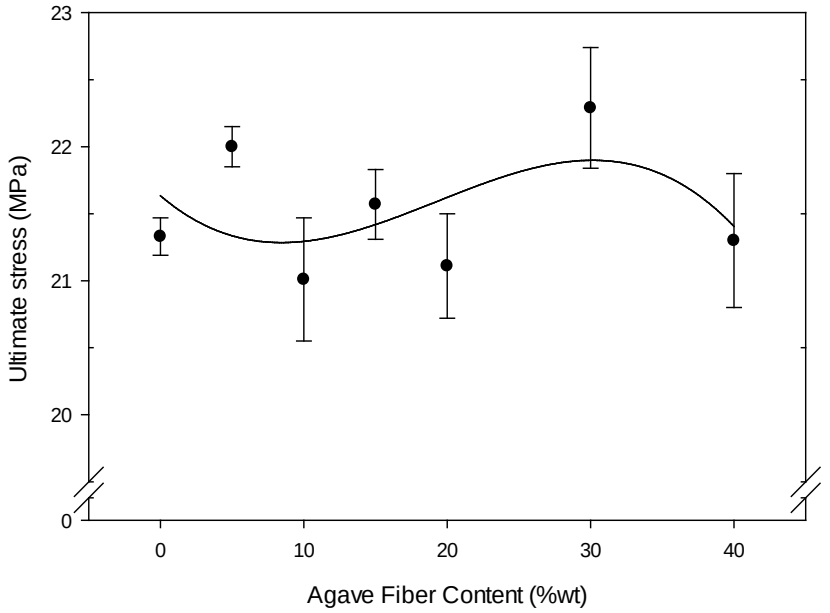

Figure 4.18 *PP/AF-B ultimate tensile strength as a function of AF content*

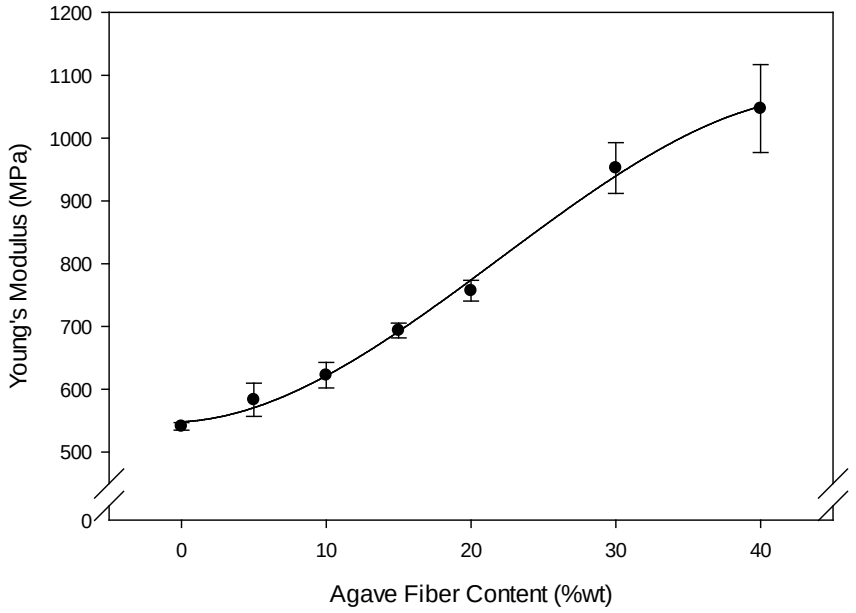

Figure 4.19 *PP/AF-B Young's modulus as a function of AF content*

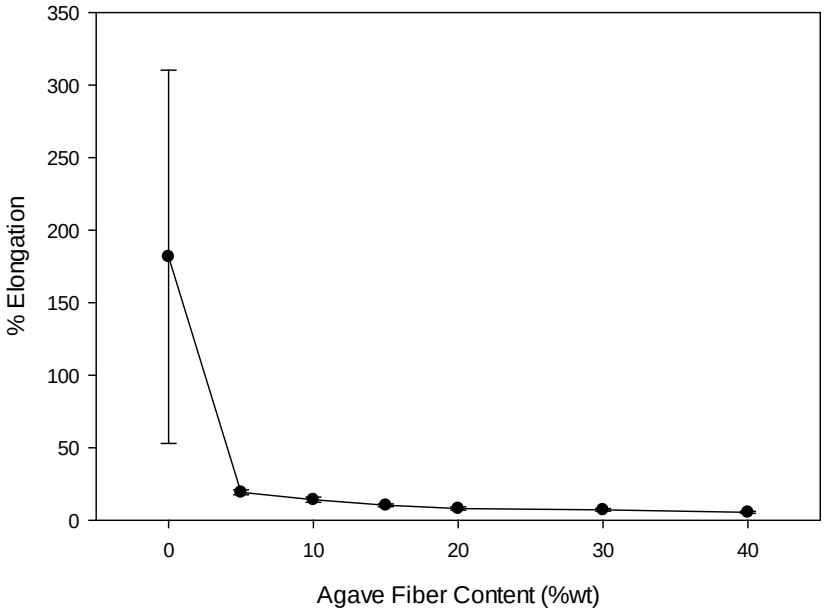

Figure 4.20 *PP/AF-B elongation as a function of AF content*

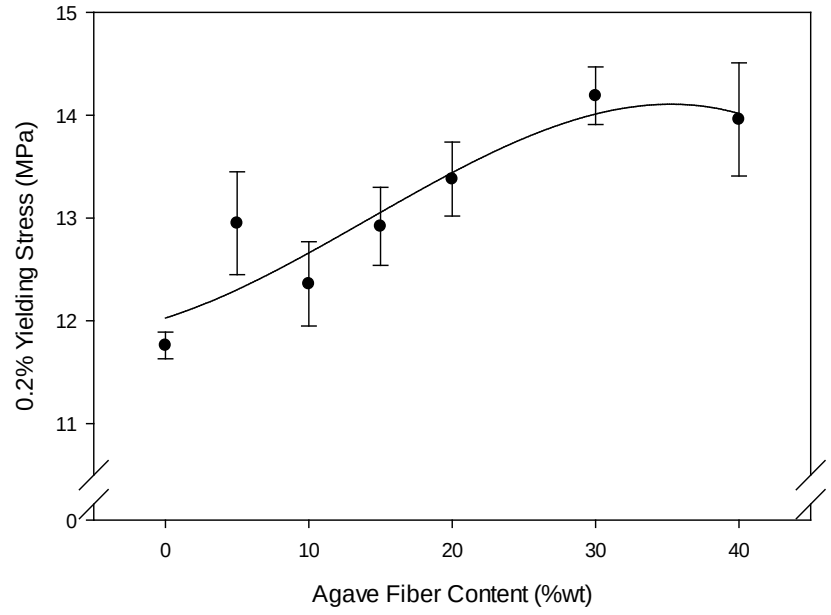

Figure 4.21 *PP/AF-B 0.2% yielding stress as a function of AF content*

In reference to the PP-r/AF-D composites, in general the ultimate stress was inversely proportional to the addition of AF-D at levels between 0 and 20% (Figure 4.22).

However, at levels above 30% the ultimate stress for washed AF-D with and without MA appeared to be comparable to the PP-r control, as seen in Figure 4.22. As previously stated, it is believed that the higher levels of AF-D encouraged fiber entanglement which promoted the increase in strength compared to lower percentages of AF-D. Overall, minimal decreases in ultimate stress were observed with a maximum decrease of 11.5% for PP-r/AF-D at 40% AF-D concentration. In general, the Young's modulus was proportional to AF-D content, with a maximum increase of 68% (compared to no AF-D) for PP-r/AF-D washed with the addition of 40% AF-D, as seen in Figure 4.23. Furthermore, the percent elongation was generally inversely proportional to the addition of AF-D, as seen in Figure 4.24. Additionally, the 0.2% yielding stress for composites with washed AF-D with and without MA was proportional to the level of AF-D, with a maximum increase of 15% at 40% AF-D concentration (compared to no AF-D). However, the yielding stresses of unwashed AF-D composites were independent of AF-D concentrations, with a decrease of 2% at 40% AF-D concentration as seen in Figure 4.25.

In general, the specific strengths were inversely proportional to the addition of AF-D at levels between 0 and 40%. However, because of the fiber entanglement mechanism previously discussed, a proportional trend is observed between 20% and 30% AF-D concentration as seen in Figure 4.26. Additionally, the specific stiffness of PP-r/AF-D composites was proportional to the addition of AF-D, with a maximum increase of 55% for PP-r/AF-D washed at 40% AF-D concentration.

In addition, impact strengths were generally inversely proportional to the annealing temperature, as seen in Figure 4.28. With no annealing, AF-D samples showed an overall decrease in impact strength, with PP-r/AF-D 90/10 washed having the smallest deficit of

7%. It is seen that as annealing temperatures were applied and increased, impact strengths were reduced in varying amounts. At 140 °C the PP-r/MA 99/1, PP-r/AF-D washed 90/10, and PP-r/AF-D unwashed samples did not provide data points as they became brittle and untestable. However, at 140 °C the PP-r/MA/AF-D washed 89/1/10 samples showed a decrease of 73% in comparison to the PP-r control.

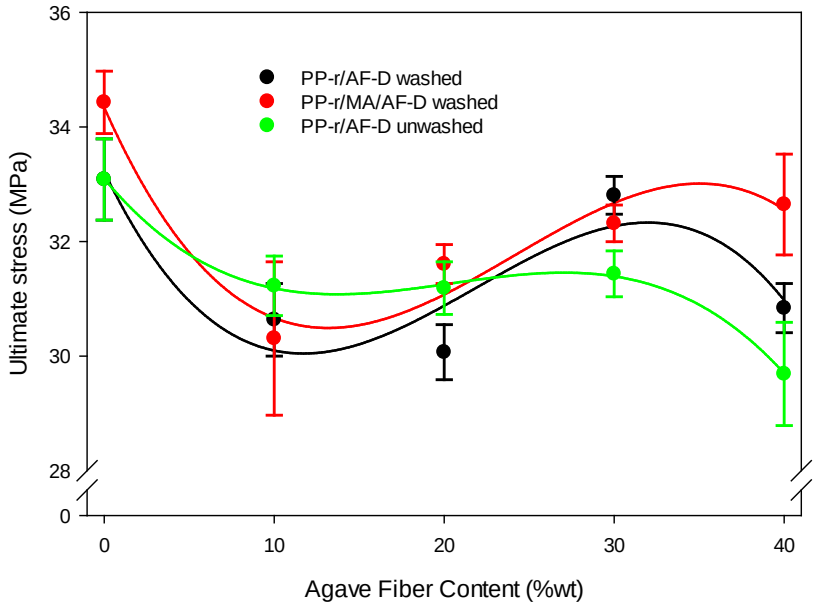

Figure 4.22 *PP-r/AF-D ultimate tensile strength as a function of AF content*

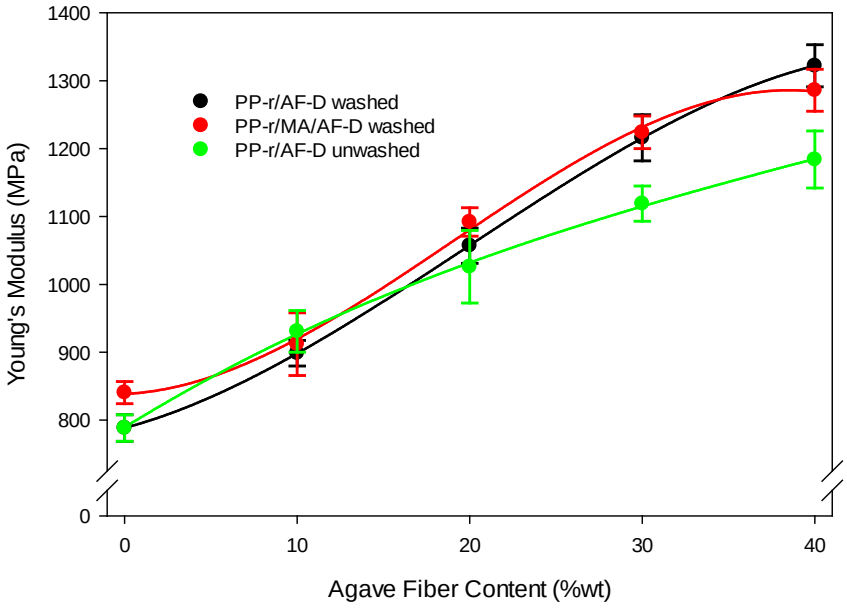

Figure 4.23 *PP-r/AF-D Young's modulus as a function of AF content*

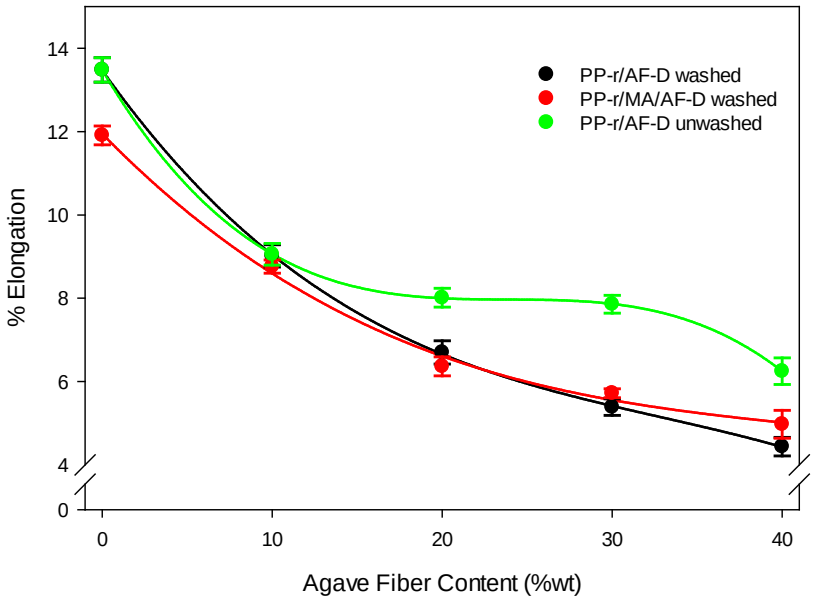

Figure 4.24 *PP-r/AF-D elongation as a function of AF content*

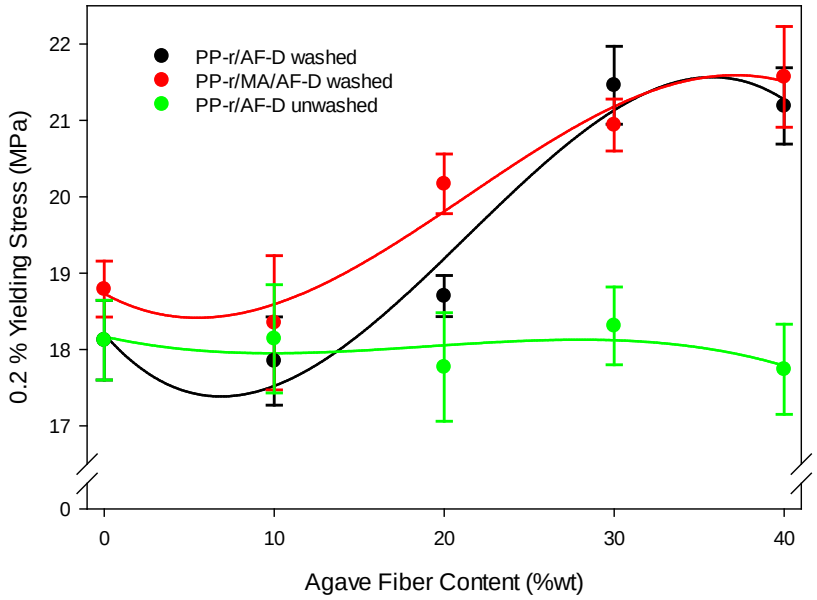

Figure 4.25 *PP-r/AF-D 0.2% yielding stress as a function of AF content*

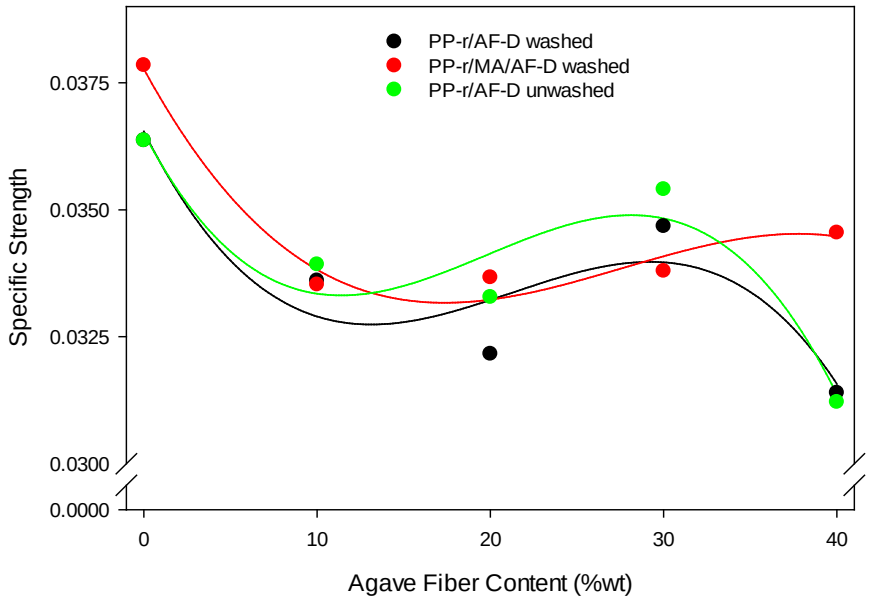

Figure 4.26 *PP-r/AF-D specific strength as a function of AF content*

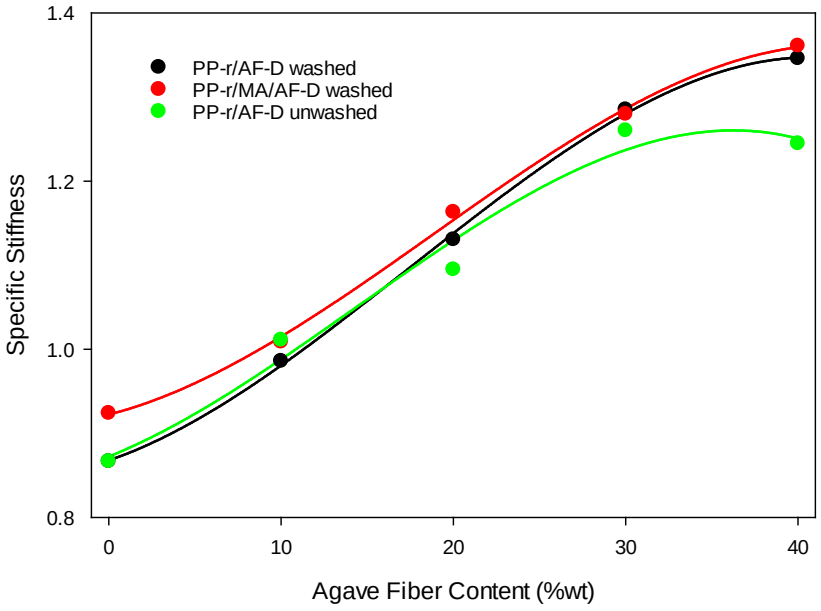

Figure 4.27 *PP-r/AF-D specific stiffness as a function of AF content*

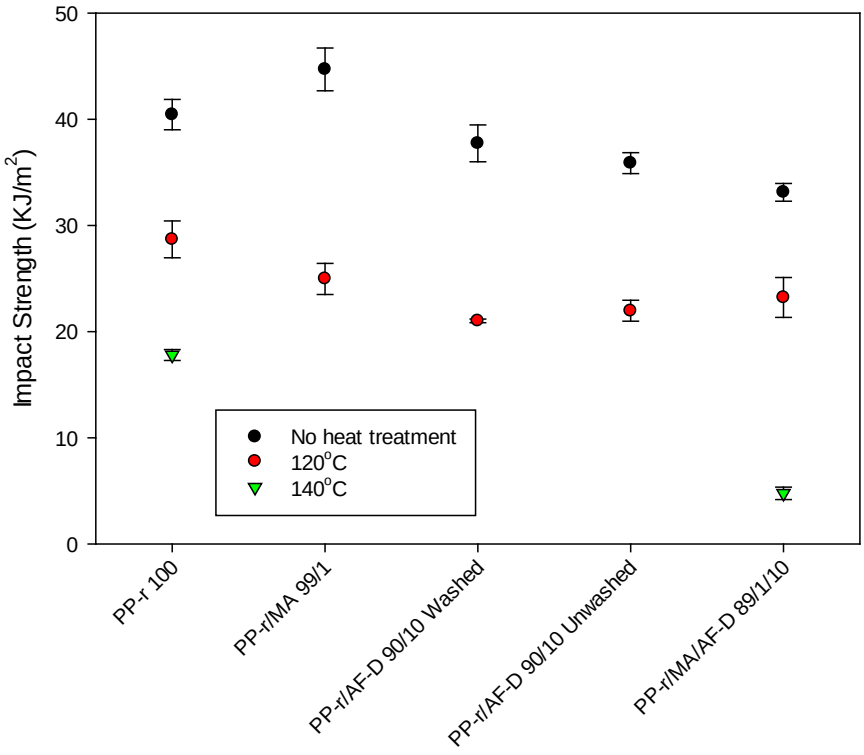

Figure 4.28 *Impact test results of thermal stress tests*

Conclusions and Recommendations

The results obtained during this study indicate that agave fiber biocomposites can be a viable alternative to currently available composites used by the automotive industry. All wash treated agave fiber biocomposites increased the 0.2% yielding strength and stiffness compared to the control groups. In addition, the odor analysis of PP/AF biocomposites showed detectable but not disturbing odors, even with untreated fiber biocomposites.

Further proof of concept was seen in bulk biocomposite material, PP/AF at 90:10 (%wt), in a successfully molded automotive HVAC component as seen in Figure 4.29. Molded biocomposite parts were reported to have a weight savings of 14%, without adverse odor, and a lower processing temperature of 177 °C in comparison to current used PP/talc 80:20 (%wt) which is processed at 232 °C.

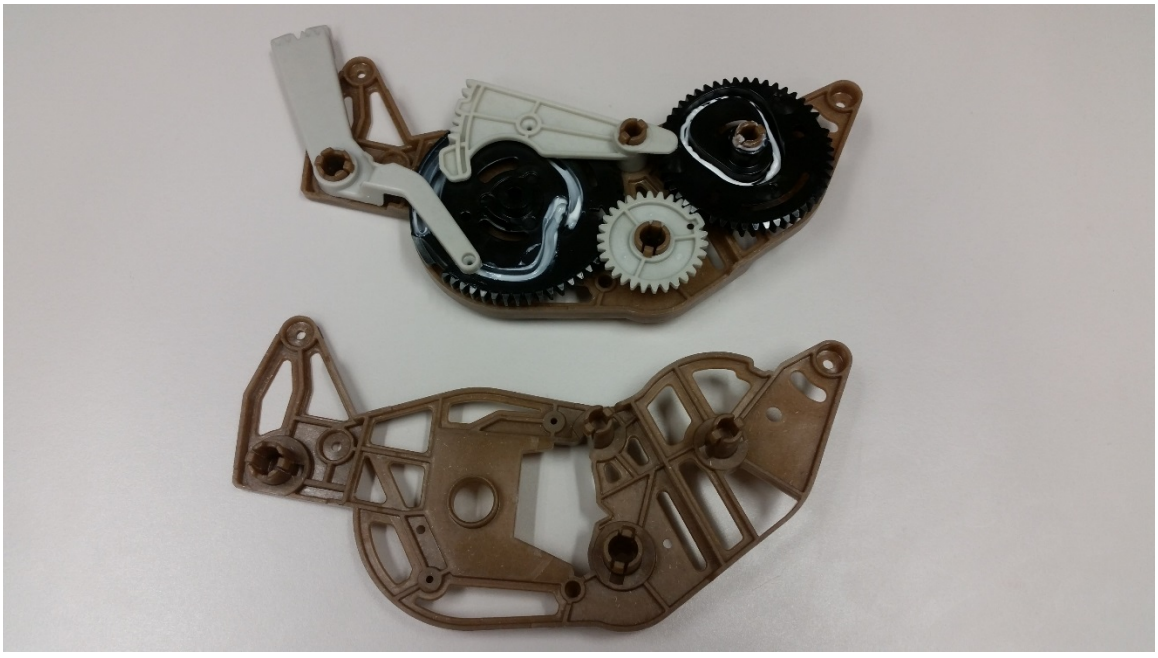

Figure 4.29 *Photograph of PP/AF-B 90:10 (%wt) injection molded HVAC component (bottom), assembled AF/PP component with gears and CAMs (above).*

Future testing incorporating the control of fiber aspect ratio could provide insight into the resulting mechanical effects. Current mechanical properties of agave fibers published incorporate fibers that have not endured the thermal and chemical effects of tequila manufacturing. Purification of tequila processed fibers remains a daunting challenge for future implementation. The incorporation of ultrasonic frequencies during fiber wash treatment should be studied to improve the feasibility and reduced cycle time needed for suitable fibers for compounding.

Any future investigation should also include a techno-economic analysis (TEA) of the production of agave fiber biocomposites to assess the cost competitiveness against current materials used in industry.

CHAPTER 5. GENERAL CONCLUSION

In this work, it was hypothesized that suitable biocomposite materials constituting lignin or agave fibers as fillers could be manufactured using thermal extrusion and injection molding processes to produce components with thermo-mechanical properties suitable for the automotive and industries alike. Biofillers continue to be a popular alternative to synthetic fillers such as e-glass based upon the highly diverse inherent qualities possessed within each and the variable mechanical properties produced.

Through this research it was determined that with appropriate pretreatments and processing conditions, successful biocomposite materials can in fact be manufactured. In addition, this research serves as a catalyst for future research by providing insight into the potential of a vast diversity of available, underutilized biofillers, such as agave fibers, indigenous to specific regions in the world that can be utilized by manufacturing operations. The continual incorporation of natural feed stocks into polymer composites remains ever vital in research pursuits to maintain sustainability in manufacturing processes.

CHAPTER 6. REFERENCES

[1] H.M.S. Iqbal, S. Bhowmik, R. Benedictus, Performance Evaluation of Polybenzimidazole Under High-Energy Radiation Environment, J. Thermophys. Heat Transf. 30 (2016) 825–830. doi:10.2514/1.T4810.

[2] Making Plastics: From Monomer to Polymer | AIChE, (n.d.). https://www.aiche.org/resources/publications/cep/2015/september/making-plastics-monomer-polymer (accessed December 26, 2017).

[3] D. Grewell, Bioplastic Container Cropping Systems: Green Technology for the Green Industry, Ames, IA, USA, 2016.

[4] W.D. Callister, D.G. Rethwisch, Fundamentals of materials science and engineering : an integrated approach, n.d. https://www.wiley.com/en-us/Fundamentals+of+Materials+Science+and+Engineering%3A+An+Integrated+Approach%2C+5th+Edition-p-9781119175483 (accessed December 26, 2017).

[5] K.L. Pickering, M.G.A. Efendy, T.M. Le, A review of recent developments in natural fibre composites and their mechanical performance, (2016). doi:10.1016/j.compositesa.2015.08.038.

[6] A.K. Mohanty, M. Misra, L.T. Drzal, Natural fibers, biopolymers, and biocomposites, Taylor & Francis Group, 2005.

[7] T.P. (Thomas P. Nevell, S.H. Zeronian, Cellulose chemistry and its applications, E. Horwood, 1985. http://apps.webofknowledge.com.proxy.lib.iastate.edu/full_record.do?product=UA&search_mode=GeneralSearch&qid=9&SID=8AsXxoJV5MsGH4growH&page=1&doc=3 (accessed December 16, 2017).

[8] M. JOHN, S. THOMAS, Biofibres and biocomposites, Carbohydr. Polym. 71 (2008) 343–364. doi:10.1016/j.carbpol.2007.05.040.

[9] K.N. Bharath, S. Basavarajappa, Applications of biocomposite materials based on natural fibers from renewable resources: a review, Sci. Eng. Compos. Mater. 23 (2016). doi:10.1515/secm-2014-0088.

[10] Standard Test Method for Tensile Properties of Plastics 1, (n.d.). doi:10.1520/D0638-14.

[11] G. I~ Niguez-Covarrubias, S.E. Lange, R.M. Rowell, Utilization of byproducts from the tequila industry: part 1: agave bagasse as a raw material for animal feeding and ®berboard production, (n.d.). https://ac.els-cdn.com/S0960852400001371/1-s2.0-S0960852400001371-main.pdf?_tid=800914e4-eeaa-11e7-b776-00000aab0f26&acdnat=1514780360_0090d96d0ab46112879e96e6420333f3.

[12] Process for preparing a thermoplastic polymer mixture based on agave fibers and residues and oxo-degradation additives for preparing biodegradable plastic articles, 2012. https://patents.google.com/patent/US20130099029A1/en (accessed April 21, 2018).

[13] M. Dubois, K.A. Gilles, J.K. Hamilton, P.A. Rebers, F. Smith, Colorimetric Method for Determination of Sugars and Related Substances, Anal. Chem. 28 (1956) 350–356. doi:10.1021/ac60111a017.

[14] FORD FLTM BO 131-03 : INTERIOR ODOR TEST, (2017) 7. https://global.ihs.com/doc_detail.cfm?&item_s_key=00497098#abstract-section (accessed September 17, 2017).

[15] P. Dalton, N. Doolittle, P.A.S. Breslin, Gender-specific induction of enhanced sensitivity to odors, Nat. Neurosci. 5 (2002) 199–200. doi:10.1038/nn803.

[16] Standard Test Method for Determining the Charpy Impact Resistance of Notched Specimens of Plastics 1, (n.d.). doi:10.1520/D6110-10.